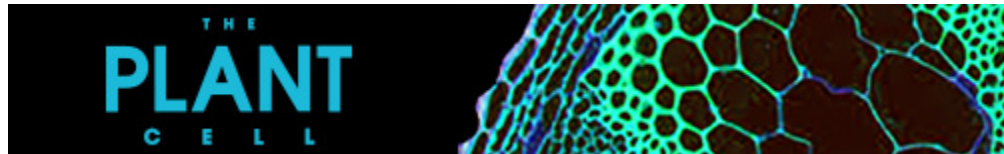


As a library, NLM provides access to scientific literature. Inclusion in an NLM database does not imply endorsement of, or agreement with, the contents by NLM or the National Institutes of Health.

Learn more: [PMC Disclaimer](#) | [PMC Copyright Notice](#)



*Plant Cell*. 2015 Sep 28;27(10):2800–2813. doi: [10.1105/tpc.15.00531](https://doi.org/10.1105/tpc.15.00531)

## Transcriptional and Hormonal Regulation of Gravitropism of Woody Stems in *Populus* [OPEN]

Suzanne Gerttula <sup>a</sup>, Matthew Zinkgraf <sup>a</sup>, Gloria K Muday <sup>b</sup>, Daniel R Lewis <sup>b</sup>, Farid M Ibatullin <sup>c,d</sup>, Harry Brumer <sup>c,e</sup>, Foster Hart <sup>f</sup>, Shawn D Mansfield <sup>f</sup>, Vladimir Filkov <sup>g</sup>, Andrew Groover <sup>a,h,1</sup>

[Author information](#) [Article notes](#) [Copyright and License information](#)

PMCID: PMC4682325 PMID: [26410302](https://pubmed.ncbi.nlm.nih.gov/26410302/)

Fundamental mechanisms associated with gravitropism in woody stems of *Populus* involve relocalization of the PIN3 auxin transporter and interacting roles for auxin, gibberellic acid, and the ARBORKNOX2 transcription factor in regulating fiber development and gravibending.

### Abstract

Angiosperm trees reorient their woody stems by asymmetrically producing a specialized xylem tissue, tension wood, which exerts a strong contractile force resulting in negative gravitropism of the stem. Here, we show, in *Populus* trees, that initial gravity perception and response occurs in specialized cells through sedimentation of starch-filled amyloplasts and relocalization of the auxin transport protein, PIN3. Gibberellic acid treatment stimulates the rate of tension wood formation and gravibending and enhances tissue-specific expression of an auxin-responsive reporter. Gravibending, maturation of contractile fibers, and gibberellic acid ([GA](#)) stimulation of tension wood formation are all sensitive to transcript levels of the Class I KNOX homeodomain transcription factor-encoding gene *ARBORKNOX2* (*ARK2*). We generated genome-wide transcriptomes for trees in which gene expression was perturbed by gravistimulation, [GA](#)

treatment, and modulation of *ARK2* expression. These data were employed in computational analyses to model the transcriptional networks underlying wood formation, including identification and dissection of gene coexpression modules associated with wood phenotypes, [GA](#) response, and *ARK2* binding to genes within modules. We propose a model for gravitropism in the woody stem in which the peripheral location of PIN3-expressing cells relative to the cambium results in auxin transport toward the cambium in the top of the stem, triggering tension wood formation, while transport away from the cambium in the bottom of the stem triggers opposite wood formation.

## INTRODUCTION

---

Gravity is a universal input that modulates plant growth and development, and various plant lineages and organs have evolved mechanisms to regulate growth and orientation relative to the force of gravity. Much of what is known about plant responses to gravity comes from studies of herbaceous annual plants wherein gravitropic responses rely on differential elongation. By contrast, lignified woody stems can no longer undergo elongation, necessitating a different solution. Instead, gravistimulated woody branches and stems undergo asymmetric radial growth to produce “reaction wood” ([Sinnott, 1952](#); [Wilson and Archer, 1977](#); [Ruelle, 2014](#)). In gymnosperms, reaction wood is termed compression wood and forms on the bottom side of the stem where it generates compressive force to push the stem upward ([Timell, 1986](#); [Ruelle, 2014](#)). In angiosperms, reaction wood is termed tension wood and forms on the upper side of gravistimulated stems where it generates a tensile force that pulls the stem upward ([Mellerowicz and Gorshkova, 2012](#)). Tension wood is produced via an increased rate of cell division in the vascular cambium and is characterized by a reduced number of water conducting vessel elements and specialized tension wood fibers containing a gelatinous cell wall layer (G-layer), which is believed to be central to force generation ([Mellerowicz and Gorshkova, 2012](#)). Tension wood fibers are capable of generating a strong contractile force, which results in negative gravitropism of the stem. The term “opposite wood” describes the wood that forms on the lower side of gravistimulated stems, but, because it is anatomically similar to “normal wood” formed by upright stems, opposite wood has received little research attention.

To comprehensively describe the gravitropism of woody angiosperm stems, four questions must be addressed: (1) What are the cells responsible for sensing gravity (i.e., graviperception), (2) what are the signals produced by gravity-sensing cells and how are they perceived by wood-forming and cambial cells, (3) how is force generated by tension wood fibers, and (4) how are the developmental processes leading to tension wood production regulated? Currently, which cells are responsible for gravity perception in woody stems is unclear. One possibility is that graviperception occurs in the shoot apex of the stem, and a signal is propagated down the stem. Alternatively, graviperception could occur within the woody stem itself. In *Populus*, starch-filled plastids that could serve as statoliths were observed in some cells of the cortex of young stems ([Leach and Wareing, 1967](#)), but no function could be ascribed to these cells in graviperception. Likewise, the mechanisms responsible for the initial graviresponse of woody stems have not been established. Similar to the graviresponses of roots and herbaceous shoots, auxin has been implicated in the graviresponse of woody stems, but conflicting conclusions from experimental ectopic application of auxin versus measurements of auxin concentrations within stems are difficult to reconcile ([Hellgren et al., 2004](#)). Other hormones, including gibberellic acid ([GA](#))

([Israelsson et al., 2005](#)) and ethylene ([Andersson-Gunnerås et al., 2003](#)), have also been implicated in tension wood formation and are potentially involved in initial graviresponse signaling, but a comprehensive understanding of how these hormones interact and affect development of secondary vascular tissues is still incomplete.

Several competing hypotheses for force generation by tension wood formation have been proposed ([Clair et al., 2006](#); [Goswami et al., 2008](#); [Mellerowicz and Gorshkova, 2012](#)) but all involve the development of fibers with specialized wall properties. Notably, the G-layer is a tertiary cell wall layer in tension wood fibers characterized by low lignin, high cellulose, and a low cellulose microfibril angle ([Norberg and Meier, 1996](#); [Clair et al., 2011](#)) that may be fundamental to force generation. Fasciclin-like arabinogalactan-encoding genes (*FLAs*) are highly upregulated during tension wood formation ([Lafarguette et al., 2004](#); [Andersson-Gunneras et al., 2006](#); [Azri et al., 2014](#)), and the *FLA* protein products have been shown to affect stem biomechanics through changes in cellulose deposition and/or cell wall structural properties ([MacMillan et al., 2010](#)). Thus, in addition to serving as molecular markers of tension wood development, *FLA* proteins could be directly involved in contributing to the altered mechanical properties of tension wood. Additionally, xyloglucan endotransglycosylase ([XET](#))-dependent linkages between the G-layer and secondary cell walls have been identified and have been implicated in the transmission of tensile stress between the G-layer and adjacent cell wall layers ([Mellerowicz et al., 2008](#); [Mellerowicz and Gorshkova, 2012](#)).

At the regulatory level, large numbers of genes are differentially expressed in tension wood, including large suites of cell wall- and hormone-related genes ([Déjardin et al., 2004](#); [Andersson-Gunneras et al., 2006](#)). Individual transcription factors have been characterized that affect wood development ([Zhong and Ye, 2013](#)), including the *Populus* Class I KNOX homeodomain protein ARBORKNOX2 (ARK2; Potri.002G113300), which is orthologous to *Arabidopsis thaliana* BREVIPEDECELLUS/KNAT1 (At4g08150) ([Chuck et al., 1996](#); [Venglat et al., 2002](#)). *ARK2* is expressed broadly in the cambial zone and lignifying cells and affects cell differentiation and expression of tension wood-related genes ([Du et al., 2009](#)). However, to date there are no transcription factors identified that specifically affect tension wood development, and the transcriptional networks underlying tension wood development remain poorly defined.

Here, we present experiments in *Populus* that identify the cells responsible for graviperception, describe changes in radial auxin transport during graviresponse, and describe the *ARK2* and [GA](#)-sensitive transcriptional networks underlying tension wood development. We suggest that the early graviresponse of auxin transport toward the cambium on the tension wood side of the stem and toward the outer cortex on the lower side of the stem sets in place a developmental switch leading to the different transcriptional and developmental outcomes of these tissues.

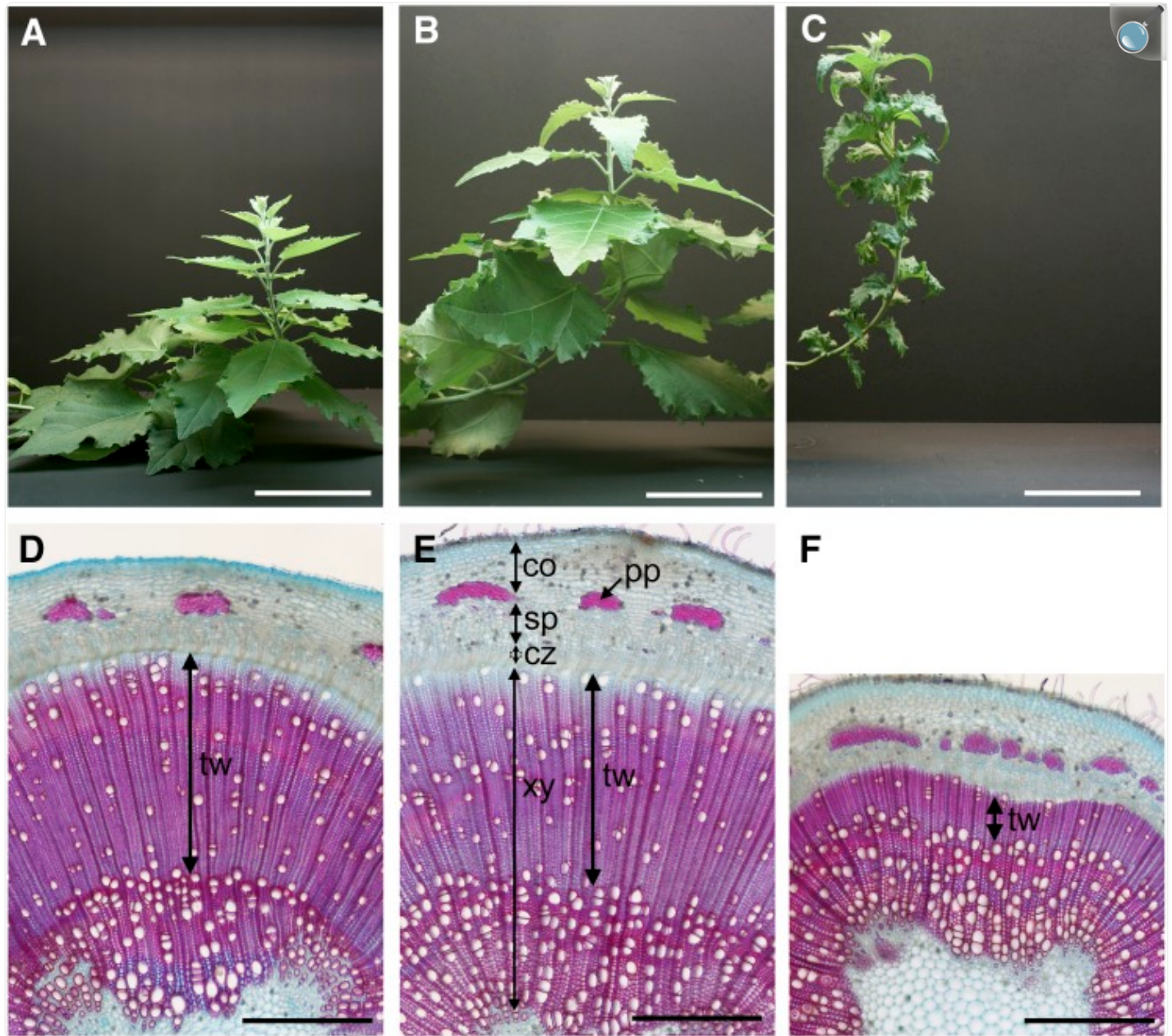
## RESULTS

---

### *ARK2* Transcript Levels Influence Fiber Development and Gravibending

To develop a comprehensive model of tension wood formation, we first focused on characterizing tension wood formation and gravitropism in *Populus* with altered *ARK2* expression. Using previously characterized genotypes ([Du et al., 2009](#)), we assayed gravibending using time-lapse videos for wild-type, *ARK2*-downregulated (miRNA-*ARK2*), and *ARK2*-overexpressing (OE-*ARK2*) *Populus* trees for a 2-week period after the trees were subjected to 90° gravistimulation ([Supplemental Movies 1 to 3](#)). miRNA-*ARK2* plants had a reduced gravibending response in comparison to the wild type, whereas OE-*ARK2* plants displayed dramatically enhanced gravibending ([Figures 1A to 1C](#); quantified in [Supplemental Figures 1A to 1C](#) and [Supplemental Movies 1 to 3](#)). Measurement of elongation growth in upright versus gravistimulated plants revealed an additional difference among the genotypes in response to gravistimulation. The wild type and OE-*ARK2* both reduced elongation growth during gravistimulation, while miRNA-*ARK2* plants did not. Surprisingly, histological comparison of stem sections showed that after 2 weeks of gravibending miRNA-*ARK2* stems had produced more tension wood fibers in comparison to the wild type, whereas the exceptional gravibending response of OE-*ARK2* was associated with fewer tension wood fibers formed ([Figures 1D to 1F](#); [Supplemental Figure 2](#) shows matched opposite wood sections). This difference was also reflected in stem diameters, with miRNA-*ARK2* and the wild type having similar diameters nearly twice that of OE-*ARK2* ([Supplemental Figure 1E](#)).

Figure 1.



[Open in a new tab](#)

*ARK2* Expression Correlates with Gravibending and Tension Wood Fiber Production.

(A) End point of 2-week time-lapse gravibending trial with miRNA-ARK2 (see [Supplemental Movies 1 to 3](#); quantified in [Supplemental Figure 1](#)).

(B) End point of 2-week time-lapse gravibending trial with the wild type (see [Supplemental Movies 1 to 3](#);

quantified in [Supplemental Figure 1](#) ).

**(C)** End point of 2-week time-lapse gravibending trial with OE-ARK2 (see [Supplemental Movies 1 to 3](#) ; quantified in [Supplemental Figure 1](#) ).

**(D)** Histology of tension wood production in miRNA-ARK2.

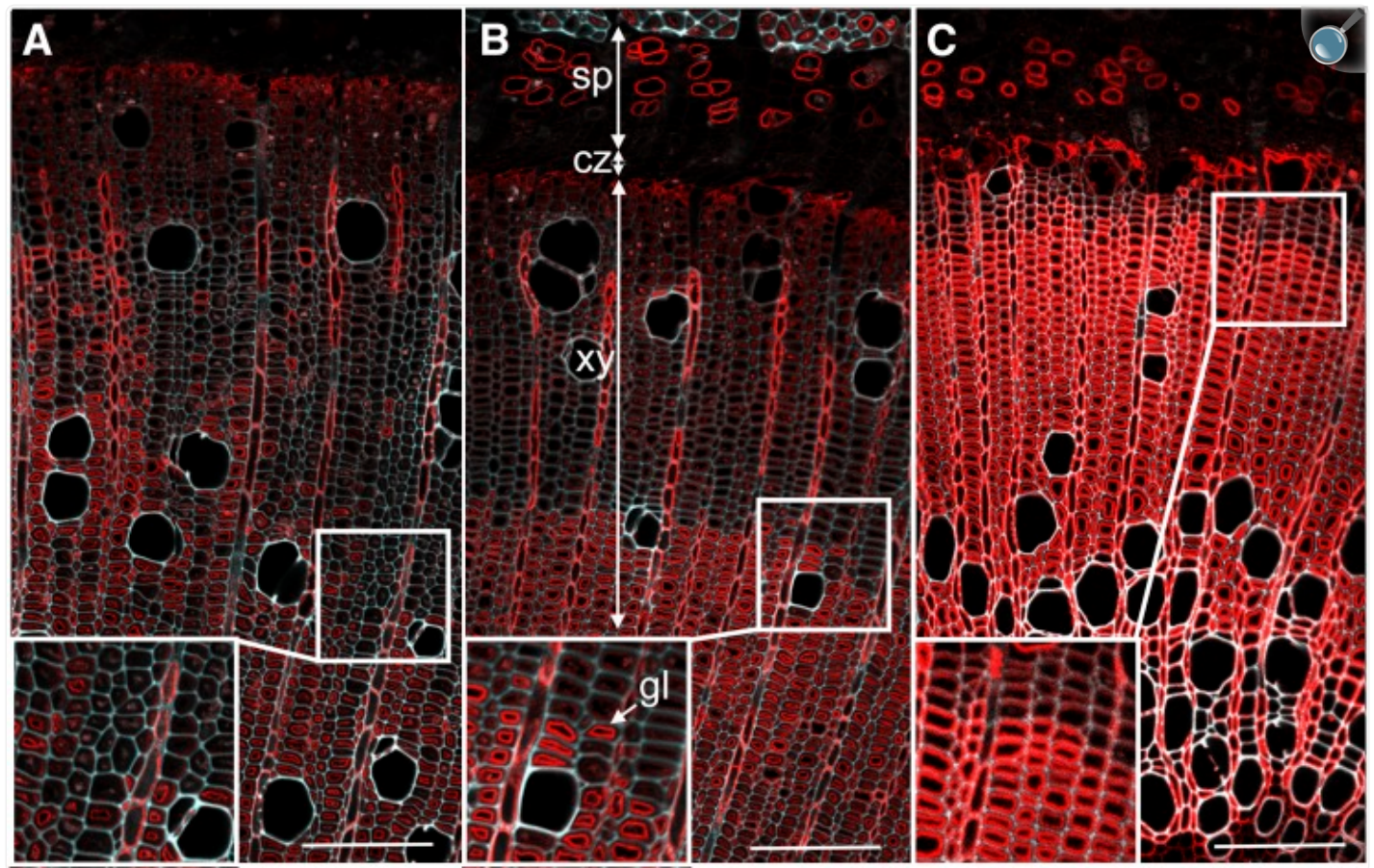
**(E)** Histology of tension wood production in wild type.

**(F)** Histology of tension wood production in OE-ARK2.

Histological staining in **(D)** to **(F)** is with phloroglucinol and astra blue (see Methods). co, cortex; cz, cambial zone; pp, phloem fibers; sp, secondary phloem; tw, tension wood; xy, secondary xylem. Bars = 10 cm in **(A)** to **(C)** and 500  $\mu$ m in **(D)** to **(F)**.

The negative correlation between number of tension wood fibers produced and gravibending among *ARK2* genotypes could reflect differences in the competency of tension wood fibers to generate force in the different genotypes. To test the hypothesis that *ARK2* might also influence the production of functional cell walls capable of generating force, each genotype was assayed for two markers that are known to be associated with maturation of functional tension wood fibers and G-layers, FLAs ([Lafargue et al., 2004](#); [Andersson-Gunneras et al., 2006](#); [Azri et al., 2014](#)), and XET ([Mellerowicz et al., 2008](#); [Mellerowicz and Gorshkova, 2012](#)). Immunolocalizations using an antibody (JIM14) recognizing arabinogalactan protein epitopes ([Knox et al., 1991](#)) (presumably including FLAs) strongly labeled the developing G-layer of tension wood fibers ([Figure 2](#)) as well as rays in all wood types ([Supplemental Figure 3](#) ). JIM14 labeling revealed distinct differences in the maturation schedule of tension wood fibers among the genotypes. OE-ARK2 trees displayed a distinct G-layer with JIM14 labeling within a few cell divisions of the cambium, while JIM14-labeled G-layers appeared much later and more erratically in miRNA-ARK2 tension wood ([Figures 2A to 2C](#)). For each genotype, the average number of tension wood fibers produced per day and the average number of tension wood fibers between the cambium and the first JIM14-labeled G-layer fiber was determined and used to calculate the average number of days required for G-layers to mature. As shown in [Table 1](#), G-layer maturation required an average of 6.6, 4.9, and 3.6 d for miRNA-ARK2, the wild type, and OE-ARK2, respectively. Thus, faster maturation of G-layers was associated with enhanced gravibending.

Figure 2.



[Open in a new tab](#)

Immunolocalizations with JIM14 Antibody to Reveal Differences in Timing of Arabinogalactan Protein Epitope Development in Developing G-Layers among *ARK2* Genotypes.

(A) miRNA-ARK2.

(B) The wild type.

(C) OE-ARK2.

In each panel, red signal originates from JIM14 labeling, while blue signal is UV autofluorescence from lignified cell walls. Inset boxes show magnified view of position where first JIM14-labeled G-layer occurs for each genotype, which is quantified in [Supplemental Figure 1D](#). cz, cambial zone; gl, G-layer; sp, secondary phloem, tw, tension wood. Bars = 200 μm.

**Table 1. Tension Wood Fiber Production and Maturation in *ARK2* Genotypes.**

Genotype	Fibers Produced <sup>a</sup>	Fibers per Day <sup>b</sup>	Fibers to G-Layer Maturation <sup>c</sup>	Days for G-Layer Maturation <sup>d</sup>
miRNA-ARK2	76.3 (SE 6.2)	5.5	36.4 (SE 6.3)	6.6
Wild type	74.4 (SE 4.7)	5.3	26.0 (SE 1.8)	4.9
OE-ARK2	33.8 (SE 2.3)	2.4	8.7 (SE 1.8)	3.6

[Open in a new tab](#)

Measurements were made for a minimum of three plants per genotype after 14 d of gravistimulation.

<sup>a</sup>Average number of tension wood fibers within a cell file.

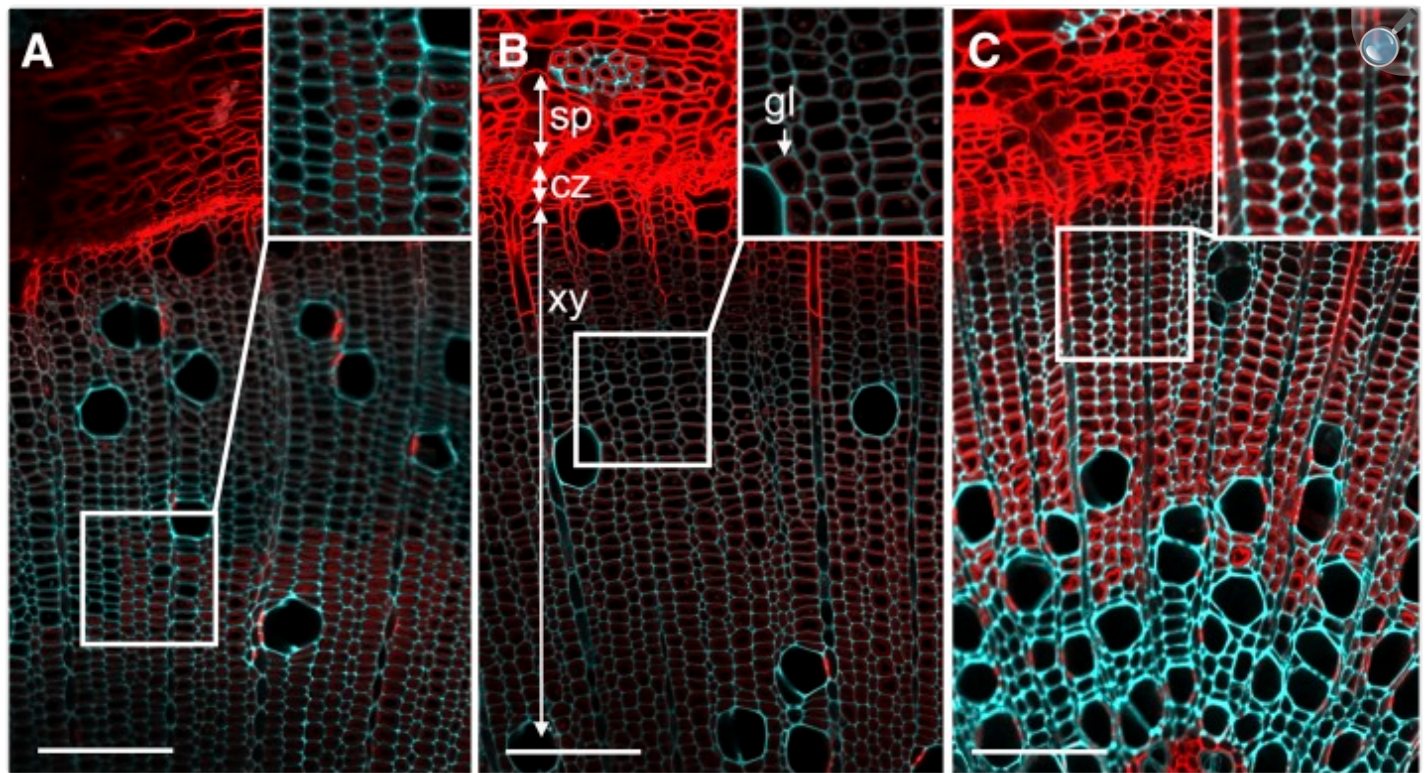
<sup>b</sup>Average number of tension wood fibers produced per day.

<sup>c</sup>Average number of tension wood fibers between the cambium and the first fiber with G-layer with JIM14 immunofluorescence signal, a proxy for G-layer maturation.

<sup>d</sup>Average number of days for tension wood fiber G-layer to mature, as assayed by JIM14 immunofluorescence.

Similarly, *in situ* imaging of XET activity using the fluorescent substrate XXXG-SR (Nishikubo et al., 2007) labeled cells of the cortex and secondary phloem in all wood types and specifically labeled G-layers in developing tension wood (Figure 3; Supplemental Figure 4 ). Similar to JIM14 labeling, OE-ARK2 G-layers were labeled within a few cells of the cambium, while miRNA-ARK2 showed variable and significantly greater numbers of cells between the cambium and fibers with labeled G-layers (Figure 3). Thus, altering *ARK2* expression manifests in dramatic differences in fiber production, fiber maturation, and stem gravibending, with gravibending performance positively correlated with the rate of G-layer maturation.

Figure 3.



[Open in a new tab](#)

In Situ Imaging of XET Activity in G-Layers to Reveal Differences in Timing of Developing G-Layers among *ARK2* Genotypes.

(A) XET activity in miRNA-ARK2.

(B) XET activity in the wild type.

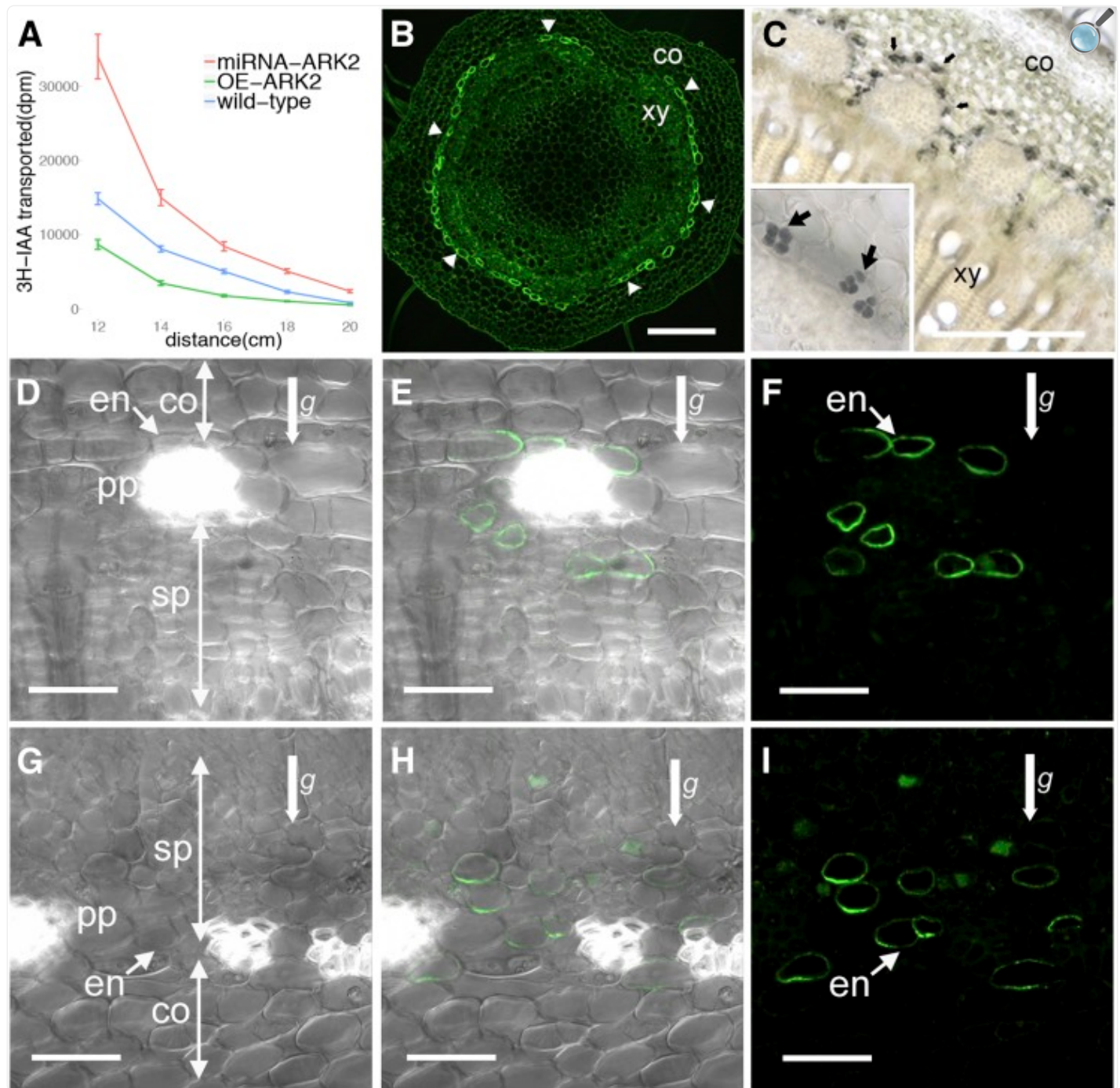
(C) XET activity in OE\_ARK2.

In each panel, red signal originates from fluorescent XET substrate XXXG-SR incorporation, while blue signal is UV autofluorescence from cell walls. Inset boxes show magnified view of position where XET labeling first occurs in G-layers for each *ARK2* genotype. cz, cambial zone; sp, secondary phloem; xy, secondary xylem. Bars = 100  $\mu$ m.

## Graviperception and Response Involves Changes in Auxin Transport

We next asked whether changes in tension wood and gravibending associated with altered *ARK2* transcript abundance could reflect differences in auxin transport. While the interpretations have varied ([Hellgren et al., 2004](#)), application of exogenous auxin to the upper surface of a *Populus* branch typically inhibits tension wood formation ([Wilson and Archer, 1977](#); [Little and Savidge, 1987](#)), raising the possibility that changes in auxin transport down and/or around the stem could influence developmental outcomes. We first measured polar (longitudinal) auxin transport from the shoot apex toward the base (basipetal) in woody stems. The greatest amount of transport was found for miRNA-*ARK2* trees, while OE-*ARK2* trees transported less auxin than wild-type controls ([Figure 4A](#)).

Figure 4.



[Open in a new tab](#)

Polar Auxin Transport Differences among *ARK2* Genotypes and Primary Graviresponse through Relocalization of PIN3 Auxin Transport Proteins.

(A) Quantification of apical to basal auxin transport in stems of *ARK2* genotypes, showing faster transport in

miRNA-ARK2 and slower transport in OE-ARK2 in comparison to wild-type controls.

**(B)** Immunolocalization with PIN3 antibody, showing labeling of the endodermis layer in the cortex of this younger, upright stem.

**(C)** Lugol staining of starch showing staining in the endodermis and secondary phloem (arrows) of cells containing starch-filled amyloplasts (inset).

**(D)** to **(F)** Immunolocalization of PIN3 in endodermal and secondary phloem cells on the tension wood side of a wild-type stem gravistimulated for 4 d. *g* indicates the gravity vector. Bright-field **(D)**, PIN3 signal **(F)**, and merged **(E)**.

**(G)** to **(I)** Immunolocalization of PIN3 in endodermal and secondary phloem cells on the opposite wood side of a wild-type stem gravistimulated for 4 d. *g* indicates the gravity vector. Bright-field **(G)**, PIN3 signal **(I)**, and merged **(H)**.

co, cortex; en, endodermis; sp, secondary phloem; xy, xylem. Bars = 500  $\mu$ m in **(B)** and **(C)** and 50  $\mu$ m in **(D)** to **(I)**.

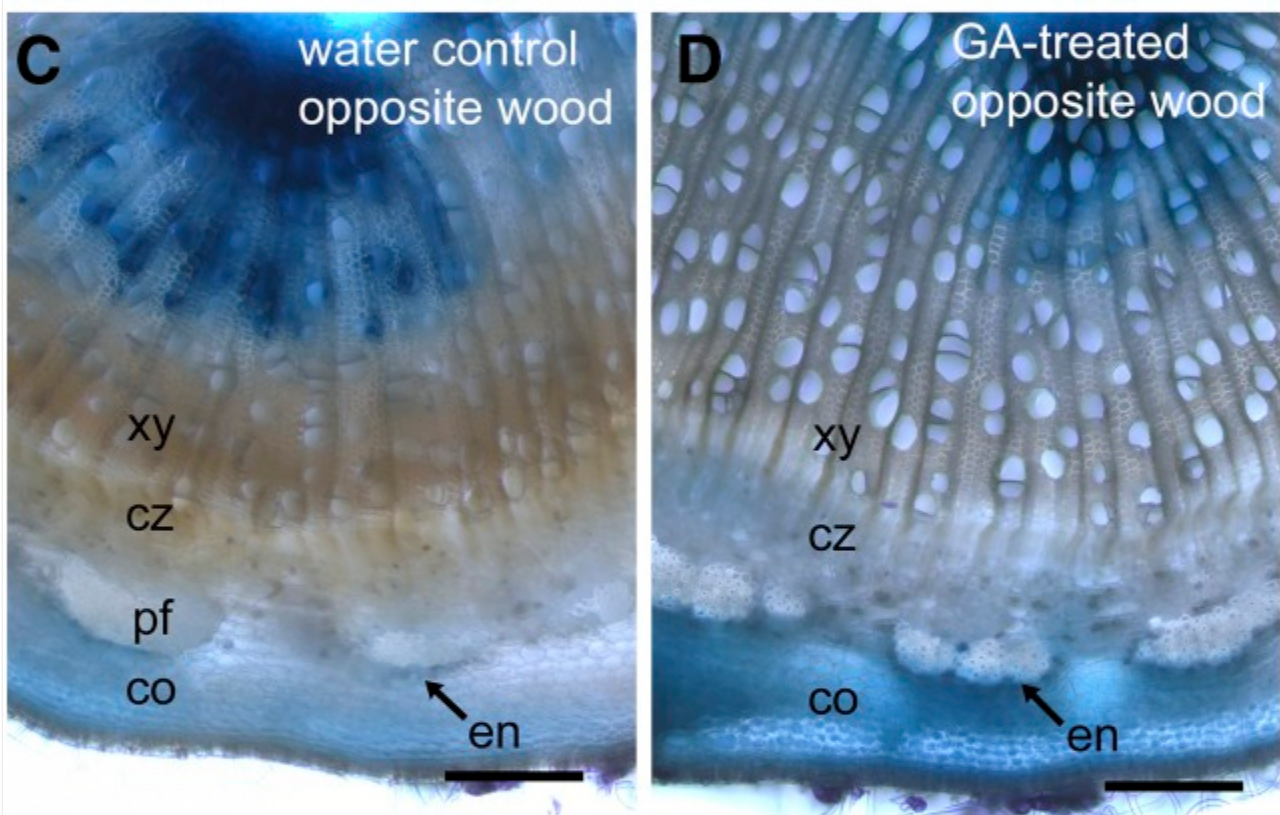
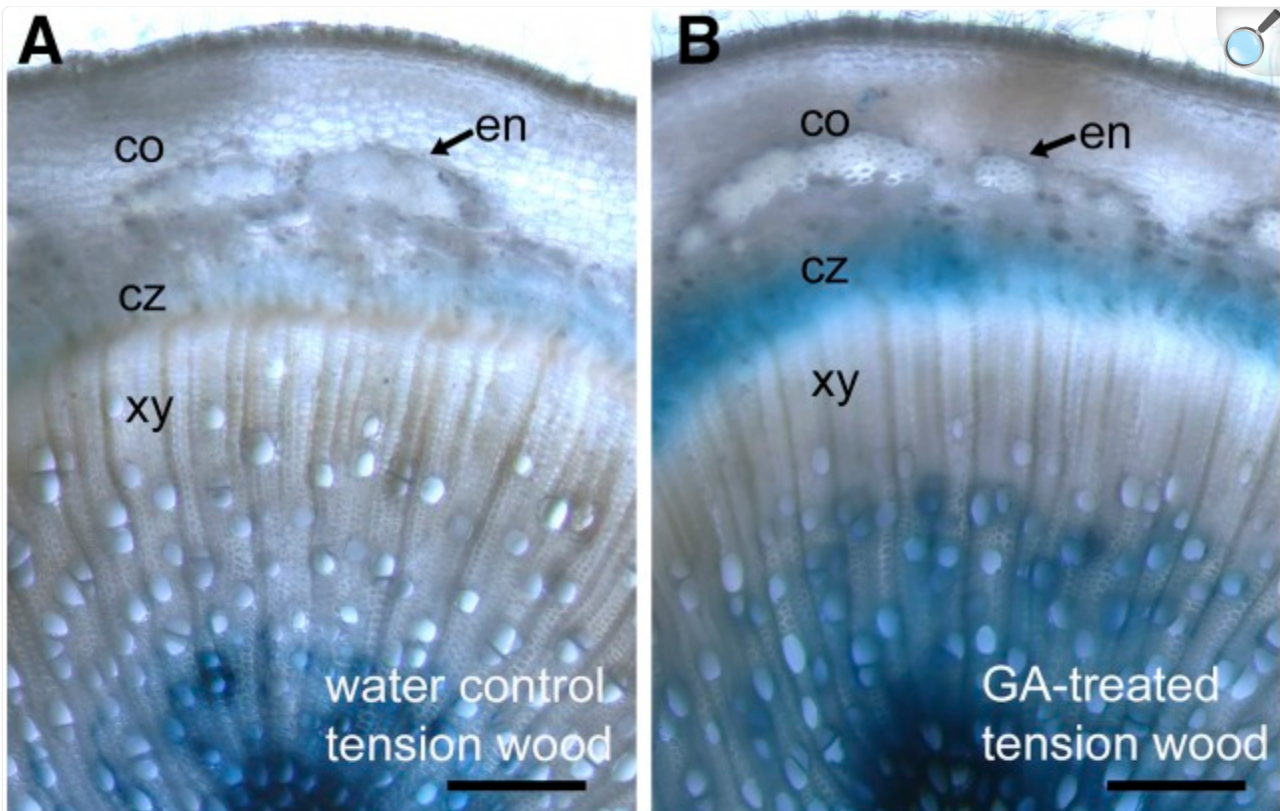
To understand how the lateral transport of auxin might be changed during graviresponse, antibodies were raised against *Populus* orthologs of the auxin polar transport protein Arabidopsis PIN-FORMED3, tested for specificity in immunoblots and control immunolocalizations (see Methods; [Supplemental Figure 5](#) ), and used in immunolocalization experiments to visualize PIN3 protein. In younger, upright stems that had recently initiated secondary growth, PIN3 showed a distinct uniform localization to the plasma membranes of endodermal cells in the inner cortex ([Figure 4B](#)), consistent with previous description of this gene's expression in the cortex in hybrid aspen (*Populus tremula*  $\times$  *tremuloides*) ([Schrader et al., 2003](#)). The endodermal cells contained starch-filled amyloplasts ([Figure 4C](#)), which sediment in response to gravity, strongly suggesting these are gravity-perceiving cells. In older stems with more extensive secondary growth, PIN3 expression could be found both in the endodermis as well as cells within the secondary phloem ([Figures 4D](#) to [4I](#)). Importantly, acquisition of PIN3 expression by cells in secondary phloem identifies a mechanism by which the woody stems can continue to perceive and respond to gravity after the loss of the endodermal layer during long-term secondary growth. Following 4 d of gravistimulation, PIN3 preferentially localized toward the ground in both the tension wood ([Figures 4D](#) to [4F](#); quantified for all genotypes in [Supplemental Figure 6](#) ) and opposite wood sides of stems ([Figures 4G](#) to [4I](#)). Because the PIN3-expressing cells are peripheral to the cambium in the radial organization of the stem, auxin would thus be predicted to be transported toward the cambial zone on the tension wood side of the stem, but toward the cortex (away from the cambium) on the opposite wood side of the stem.

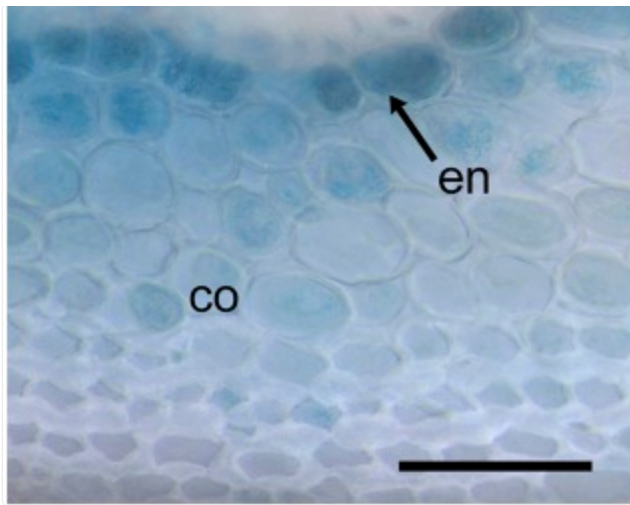
Thus, lateral auxin transport toward the ground by PIN3-expressing cells could elicit differential growth responses of the cambium to gravistimulation on the upper (tension wood) versus lower (opposite wood) sides of the stem.

## [GA](#) Potentiates Auxin Response and *ARK2*-Dependent Fiber Production

Previous reports have identified [GA](#) metabolism genes as direct targets of KNOX transcription factors ([Bolduc and Hake, 2009](#); [Hay and Tsiantis, 2010](#)), and [GA](#) has been shown to affect the differentiation of fibers during wood development ([Eriksson et al., 2000](#); [Mauriat and Moritz, 2009](#)). The effect of [GA](#) treatment on auxin responses during graviresponse and tension wood formation was assayed through expression of a DR5:GUS construct that reports auxin response ([Spicer et al., 2013](#)) in trees subjected to a soil drench [GA](#) treatment (29 μm in soil; see Methods). In upright trees, DR5:GUS expression was detected in the cambial zone of trees after [GA](#) treatment but not in control trees ([Supplemental Figure 7](#)). In untreated trees gravistimulated for 4 d, the GUS reporter staining was weakly apparent in the cambial zone of the tension wood side of the stem, while stronger staining was apparent in the cortex in the opposite wood side of the stem ([Figures 5A](#) and [5C](#)). This staining pattern was enhanced in response to [GA](#) treatment ([Figures 5B](#) and [5D](#)). Notably, the endodermis appeared to be a boundary for GUS staining in the opposite wood side of the stem ([Figure 5E](#)), consistent with endodermal PIN3 directing auxin flow toward the cambium on the tension wood side and toward the cortex on the opposite wood side of the stem after gravistimulation. These results also show that increased [GA](#) levels potentiate the auxin responsiveness of these same tissues and are reminiscent of [GA](#) regulation of PIN protein stability and localization that has been described for root gravitropism in *Arabidopsis* ([Willige et al., 2011](#); [Löfke et al., 2013](#)).

**Figure 5.**





[Open in a new tab](#)

#### Effects of GA on Auxin Response Measured by DR5:GUS.

Auxin response assayed by the DR5:GUS reporter for tension wood and opposite wood for water control or GA-treated trees. co, cortex; cz, cambial zone; en, endodermis; pf, phloem fibers; xy, secondary xylem. Bars = 200  $\mu\text{m}$  in (A) to (D) and 50  $\mu\text{m}$  in (E).

(A) Water control, tension wood.

(B) GA-treated, tension wood.

(C) Water control, opposite wood.

(D) GA-treated, opposite wood.

(E) DR5:GUS expression in the endodermis of opposite wood for a water control tree.

The effect of GA on tension wood fiber development was tested by treating wild-type, OE-ARK2, and miRNA-ARK2 trees with a soil drench of either water (control) or 29  $\mu\text{M}$  GA. Trees treated with GA showed an increase in gravibending response in comparison to controls ([Supplemental Figure 7C](#)). GA modestly increased the number of tension wood fibers formed after 2 weeks gravibending for wild-type and OE-ARK2 trees ([Supplemental Figure 7D](#)). By contrast, the number of fibers produced by control and GA-treated miRNA-ARK2 trees did not vary and was similar to that found in GA-treated wild-type trees ([Supplemental Figure 7D](#)). The maturation of G layers as assayed by JIM14 labeling ([Supplemental Figure 8](#)) and XET labeling ([Supplemental Figure 9](#)) showed similar trends, with

[GA](#) treatment modestly increasing the rate of maturation in the wild type and OE-ARK2 but having no significant effect in miRNA-ARK2. Together, these observations suggest that [GA](#) stimulates tension wood fiber production and that this effect is sensitive to *ARK2* levels, consistent with negative regulation of [GA](#) levels by *ARK2* and elevated endogenous levels of [GA](#) in miRNA-ARK2.

## Transcriptional Networks Associate Gene Expression with Wood Development

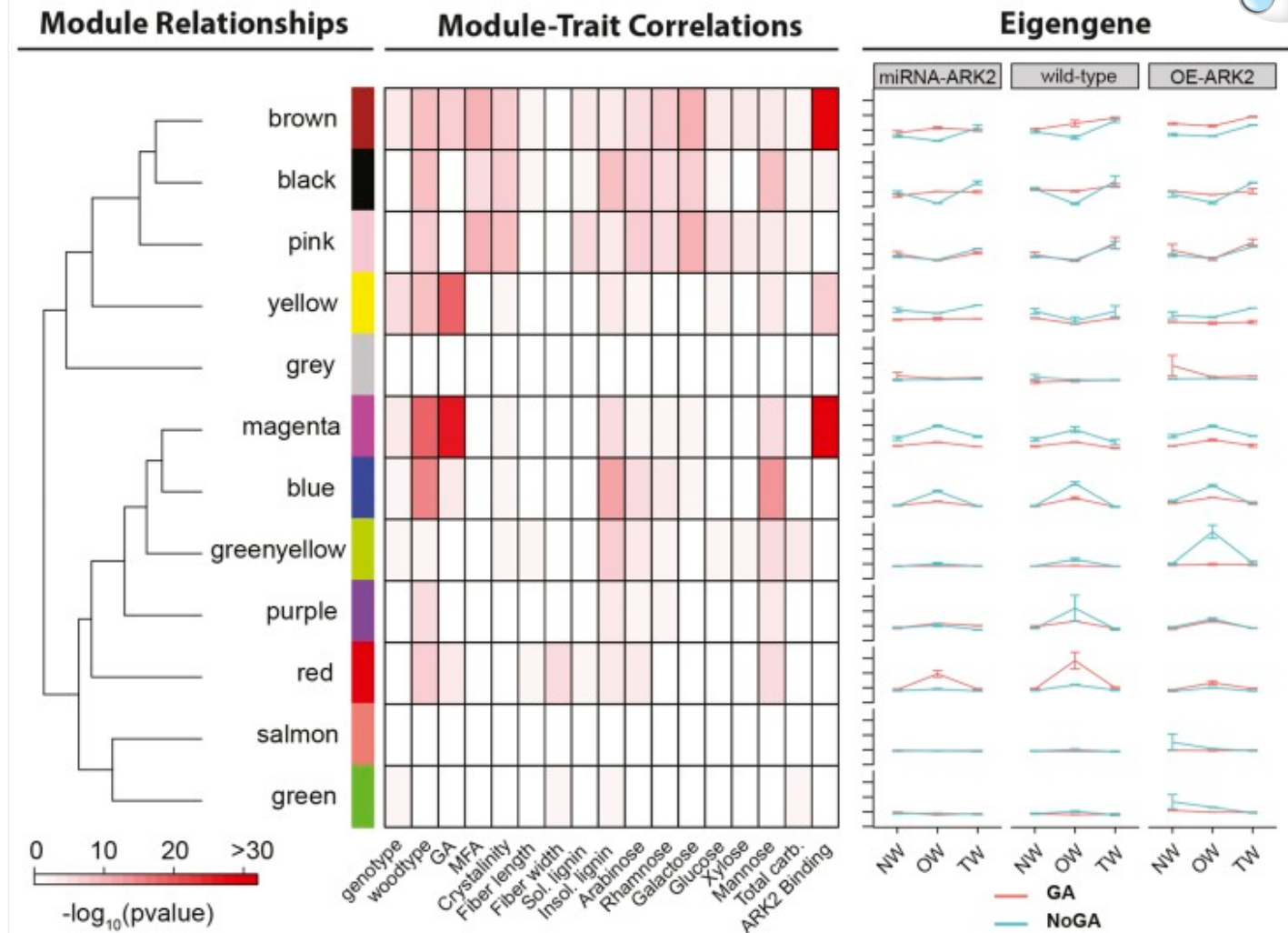
In a final set of experiments, computational approaches were used to model the transcriptional regulation of tension wood development using genome-wide transcriptome data from trees in which gene expression had been perturbed by gravistimulation, [GA](#) treatment, and modulation of *ARK2* expression. A full factorial experiment was performed with trees of wild-type, miRNA-ARK2, and OE-ARK2 genotypes subjected to either [GA](#) or a control (mock) treatment and then either gravistimulated or allowed to remain upright. After 2 d, developing xylem was lightly scraped from both tension wood and opposite wood from gravistimulated trees after debarking or from two opposing sides of the upright trees and subjected to RNA sequencing (see Methods). Differential transcript abundance was calculated for comparisons of wood types, genotypes, and [GA](#) treatment, with relatively large numbers of genes showing differential expression in each comparison ([Supplemental Figure 10](#)). Notably, comparison of transcript levels across wood types revealed a massive reprogramming of gene expression in opposite wood, with the majority of differentially expressed genes being upregulated in that tissue ([Supplemental Figure 10](#)).

Next, weighted gene correlation network analyses ([Langfelder and Horvath, 2008](#)) were performed to define modules (clusters) of coexpressed genes whose transcript levels covaried across samples. Modules were initially characterized for robustness by repeated random sampling and recalculation of modules ([Supplemental Figure 11A](#)) and by calculating coexpression relationships among all combinations of modules ([Supplemental Figure 11B](#)). Modules were next annotated to describe the expression and functional properties of genes within modules and their correlations to traits of interest ([Supplemental Data Set 1](#)). As visualized by eigengene values (the first principal component of transcript profiles) for each module ([Figure 6A](#)), variation in transcript levels across wood types was the primary factor in defining gene coexpression modules, followed by [GA](#) treatment and to a lesser extent *ARK2* genotype. Coexpression relationships across modules ([Supplemental Figure 11B](#)) were evident based on eigengene values; for example, the sister brown, black, pink, and yellow modules were characterized by tension wood expression, while the sister magenta, blue, green-yellow, purple, and red modules were characterized by opposite wood expression ([Figure 6A](#)). Correlations were calculated between each gene module and phenotypic traits, including *ARK2* genotype, wood type, [GA](#) treatment, and wood phenotypes (microfibril angle, cellulose crystallinity, fiber morphology, lignin, and carbohydrates; [Supplemental Figure 12](#)). Interestingly, significant correlations were found between each trait and at least one gene module ([Figure 6A](#)). All five gene modules with significant correlations to [GA](#) treatment (brown, yellow, magenta, blue, and red) were also correlated with *ARK2* genotype, and four were also correlated with wood type. However, of the three modules (brown, black, and pink) showing significant correlations with microfibril angle and cellulose crystallinity traits associated with functional tension wood fibers, only brown showed significant correlation with [GA](#), suggesting

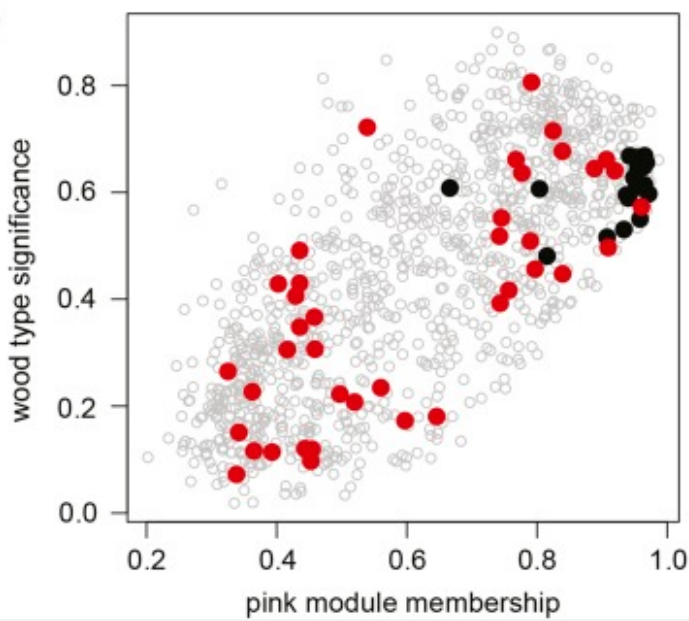
that the role of [GA](#) may be more closely tied to stimulation of tension wood fiber production than regulation of cell wall properties. Modules were also identified that had significant enrichment for specific Gene Ontology ([GO](#)) categories ([Supplemental Figure 11C](#) and [Supplemental Data Set 2](#) ), allowing further insight into the functional properties of modules. For example, each of the modules characterized by tension wood expression had distinct [GO](#) enrichment profiles, with the brown module characterized by enrichment for “localization,” the black module enrichment for replication, the pink module for hormone, auxin, and cell wall, and yellow module for cell wall, meristem, and localization [GO](#) terms. Together, these annotations can be used to develop and test new hypotheses regarding the function of *ARK2*, response to [GA](#), or tension wood development through the identification and further dissection of gene modules of interest, as illustrated below.

Figure 6.

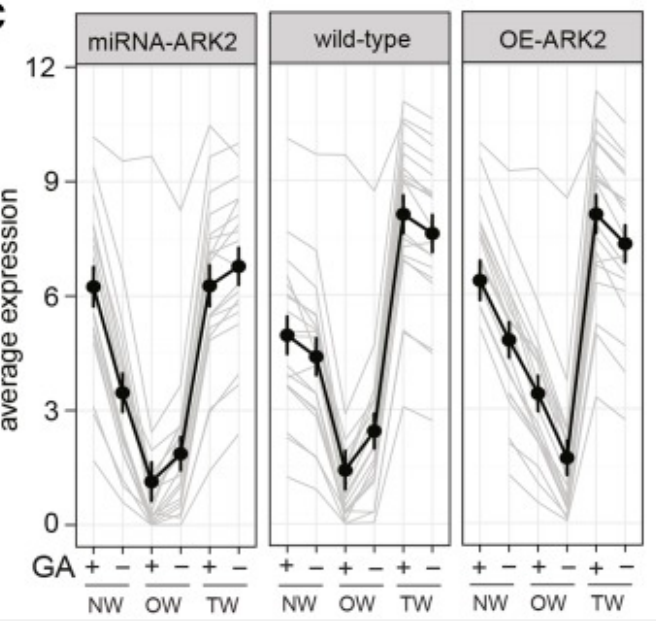
A



B



C



Transcriptional Network Regulating Wood Formation and Associations with Phenotypes.

**(A)** Dendrogram showing relationships of gene modules (colors), correlations of individual gene modules with phenotypes, and module eigengene expression across *ARK2* genotypes (miRNA, miRNA-*ARK2*; OE, OE-*ARK2*) and wood types (NW, normal wood; OW, opposite wood; TW, tension wood) in response to [GA](#) treatment.

**(B)** Plot of genes in the pink module for differential expression across wood types (*y* axis) and module membership/connectivity (*x* axis). Black data points are *FLA* genes. Red data points are transcription factor-encoding genes.

**(C)** Line graphs showing the average (bold line) and individual transcript levels (gray lines) of the 19 *FLA* genes in the pink module across *ARK2* genotypes and wood types in response to [GA](#) treatment.

*ARK2* was placed in the blue module and showed modest connectivity within that as well as several other modules ([Supplemental Data Set 1](#)). *ARK2* binding was recently evaluated, genome-wide, using chromatin immunoprecipitation sequencing ([ChIP-seq](#)) ([Liu et al., 2015](#)). Here, four modules (brown, black, yellow, and magenta) showed enrichment for genes bound by *ARK2* ([Figure 6A](#)). All of the *ARK2* binding enriched modules also showed correlations with wood type and three showed correlations with [GA](#) treatment (brown, yellow, and magenta) and/or genotype (brown, yellow, and magenta), reflecting our experimental data indicating that *ARK2* and [GA](#) interact and have major effects on wood development. Together, the modest connectivity of *ARK2* and binding to large numbers of genes of diverse function suggest that this transcription factor does not act as a “master regulator.” Instead, these data are more consistent with *ARK2* acting as a transcription factor that influences and potentially integrates multiple development-related processes, including cell wall development and hormone-related functions.

As an example of how coexpression modules can be further dissected to understand tension wood development, we focused on the pink module, which is characterized by expression in tension wood across all genotypes ([Figure 6A](#)) and has correlations with cellulose crystallinity and microfibril angle that are correlated with tension wood development and function ([Figure 6A](#); [Supplemental Figure 12](#)). When genes within this module were plotted relative to their correlation with wood type and module membership (a measure of connectivity within the module), several *FLA*-like genes that are markers of tension wood development ([Lafargue et al., 2004](#); [Andersson-Gunneras et al., 2006](#); [Azri et al., 2014](#)) and reflected in our JIM14 labeling of tension wood G-layers ([Figure 2](#)) were identified in the upper quartile of both traits (black data points in [Figure 6B](#); [Supplemental Data Set 1](#)), suggesting this module contains genes

directly relevant to differentiating tension wood. Strikingly, the transcription factors within the module (red data points in [Figure 6B](#)) include 11 MYB, 6 NAC, and 2 KNOX transcription factors incorporating orthologs of characterized genes known to regulate meristematic growth ([Zhou et al., 2009](#)), fiber development, and/or secondary cell wall biosynthesis in Arabidopsis (e.g., MYB52 and MYB85, KNAT6 and KNAT7, BLH4 and VND1; [Belles-Boix et al., 2006](#); [Ragni et al., 2008](#); [Zhong et al., 2008](#); [Liu et al., 2014](#); [Taylor-Teeple et al., 2015](#)). These serve as excellent candidates for regulating the expression of other genes within the module ([Supplemental Data Set 1](#) ), which include genes central to graviresponse and tension wood formation, including auxin (e.g., *PIN1* and *PIN3* orthologs), [GA](#) biosynthesis (*GA20-Oxidase*), and cell wall biosynthesis (e.g., *IRREGULAR XYLEM* genes and 19 *FLAs*). Finally, potential radial signaling-related genes with high wood type and module membership also reside in the pink module, including CLE13-like and SCARECROW-like 8.

## *FLA* Expression Reveals Differential [GA](#) Response across Wood Types and ARK Genotypes

Looking in detail at the expression of the *FLAs* within the pink module, three trends are apparent ([Figure 6C](#)): (1) *FLA* transcript levels are highest in tension wood and lowest in opposite wood in all genotypes ( $t = 15.304$ ,  $df = 18$ , P value = 4.603e-12), (2) *FLA* transcript levels are lower in the tension wood of miRNA-ARK2 than the wild type or OE-ARK2 ( $t = -12.764$ ,  $df = 18$ , P value = 9.284e-11), and (3) *FLA* transcript levels show *ARK2*-dependent differential expression in response to [GA](#) treatment in tension wood and opposite wood (P values < 0.001). Specifically, *FLA* levels are induced by [GA](#) treatment in tension wood for OE-ARK2 and the wild type, but miRNA-ARK2 shows repression of *FLA* transcript levels by [GA](#). These results are reminiscent of the responses of these same genotypes to [GA](#) treatment with regards to maturation of G-layers as assayed by JIM14 immunolocalization ([Supplemental Figure 8](#) ). Additionally, *FLA* levels are repressed by [GA](#) in opposite wood of wild-type and miRNA-ARK2 trees, but increased by [GA](#) in opposite wood of OE-ARK2. Thus, the response to [GA](#) is different across both wood types and *ARK2* genotypes, potentially revealing a developmental switch set in place by the initial graviresponse and radial auxin transport that is sensitive to *ARK2* transcript levels.

## DISCUSSION

---

The negative gravitropism of woody angiosperm stems is fundamentally different from that of herbaceous stems. The herbaceous stem achieves negative gravitropism through differential growth on the bottom of the stem that pushes the stem upward. By contrast, the woody stem undergoes differential growth on the top of the stem to produce tension wood that pulls the stem upward with contractile forces ([Sinnott, 1952](#); [Wilson and Archer, 1977](#); [Ruelle, 2014](#)). In this study, we identified key regulatory mechanisms involved in negative gravitropic responses in woody *Populus* stems, including the cells responsible for graviperception, the initial graviresponse via relocalization of the PIN3 auxin transporter, and interacting roles for auxin, [GA](#), and the *ARK2* transcription factor in regulating fiber development and gravibending.

Using *Populus* as a model species, we found that graviperception likely occurs directly in the woody stem in specialized cells containing starch-filled amyloplasts that sediment toward the ground. These cells are further defined by expression of the auxin transport protein, PIN3, which relocates toward the ground during gravistimulation. The PIN3-expressing cells are initially found in the endodermis, similar to what has been found in *Arabidopsis* ([Friml et al., 2002](#)) and other herbaceous stems, but later in development cells within the secondary phloem acquire PIN3 expression and possess amyloplasts. Thus, even though the endodermis is eventually lost during the outward expansion of the cortex during secondary growth, older woody stems can continue to sense gravity as new cells within the secondary phloem acquire PIN3 expression. Importantly, the reorientation of PIN3 toward the ground in gravistimulated woody stems would be predicted to have different outcomes on auxin transport in the top versus bottom of the stem. Because of the radial organization of the stem, on the top (tension wood side) of a gravistimulated stem PIN3 orientation is toward the cambium and center of the stem, whereas in the bottom (opposite wood side) of the stem PIN3 orientation is toward the cortex and periphery of the stem. These orientations are reflected in expression of a DR5:GUS reporter in our experiments, which shows preferential cambial expression on the top and cortical expression in the bottom of gravistimulated stems. This lateral auxin transport and response represents the earliest known graviresponse of woody stems and provides an obvious initial mechanism triggering the different developmental fates of xylem tissues that develop on the top (tension wood) versus bottom (opposite wood) of the gravistimulated stem.

Our results concerning the location of graviperceptive cells and radial auxin transport in the tension wood versus opposite wood side of gravistimulated stems may also help in understanding previous, apparently conflicting, research results. Exogenous application of auxin to the upper surface of a leaning stem resulted in inhibition of tension wood formation ([Cronshaw and Morey, 1968](#)), while application of antiauxins induces tension wood ([Cronshaw and Morey, 1965](#)). These results led to the proposition that low auxin levels in the cambium induce tension wood development. However, direct measurement of auxin in gravistimulated *Populus* stems did not detect lower levels in cambia producing tension wood in comparison to cambia in upright trees; in fact, significantly lower auxin levels were found for cambia producing opposite wood ([Hellgren et al., 2004](#)). Our results would suggest that exogenous auxin application could likely mimic the conditions in the opposite wood side of the stem, where auxin transport would result in higher auxin and auxin response in the cortex than the cambial zone. The lower levels of auxin reported for the cambial region on the bottom of the stem (producing opposite wood) are consistent with auxin transport away from the cambium, as suggested by PIN3 localization and the DR5:GUS reporter in our experiments. However, the previous observation that levels of auxin in cambia producing tension wood are not higher than those for cambia producing normal wood ([Hellgren et al., 2004](#)) may indicate that it is not necessarily the absolute concentration of auxin in the cambial zone that determines the type of wood produced by the cambium. Instead, the relative amounts of auxin across the radially arranged secondary vascular tissues or differential sensitivity of auxin across these tissues may be more important. It is also possible that auxin itself is not directly inducing the different developmental outcomes at the cambial zone, but rather is involved in generating the signals that more directly elicit the developmental changes.

Auxin is not the only hormone influencing wood development, and we found [GA](#) to be an important hormonal regulator

of tension wood, capable of stimulating fiber production and gravibending. Interestingly, previous authors have also attributed positive regulation of tension wood development to [GA](#) and speculated, based on gene expression and direct measurement of [GA](#), that [GA](#) precursors may be synthesized in the phloem and transported to the xylem, potentially through rays ([Israelsson et al., 2005](#)). The rays interconnect the secondary xylem (wood), cambium, and secondary phloem ([Lev-Yudan and Aloni, 1995](#)) and, although their role in development is poorly understood, could be important in radial signaling in woody stems. For example, radial movement of auxin from the primary vascular bundles to the cambial zone has been demonstrated in *Populus* and likely involves the rays ([Spicer et al., 2013](#)). Strikingly, ectopic application of [GA](#) can induce tension wood formation ([Nakamura et al., 1994](#)), making it a good candidate for a more direct signal controlling differentiation downstream of auxin. We found that transcriptional responses to [GA](#) treatment were sensitive to *ARK2* transcript levels and that, in contrast with wild-type or *ARK2* overexpressing trees, trees with reduced *ARK2* transcript abundance failed to produce additional tension wood fibers in response to [GA](#) treatment. These results would be consistent with the idea that decreased levels of *ARK2* transcript are associated with elevated [GA](#) levels, similar to previous work in herbaceous species that have demonstrated a direct positive regulation of [GA](#) catabolism-related and negative regulation of [GA](#) biosynthesis-related genes by Class I KNOX transcription factors ([Sakamoto et al., 2001](#); [Jasinski et al., 2005](#); [Bolduc and Hake, 2009](#)). In addition, we found that [GA](#) potentiated the expression of the auxin-responsive DR5:GUS reporter in gravistimulated stems. This result is reminiscent of previous studies in trees showing [GA](#) stimulation of polar auxin transport during wood development ([Bjorklund et al., 2007](#)) and of reports of [GA](#) regulation of PIN protein stability and localization during root gravitropism in *Arabidopsis* ([Willige et al., 2011](#); [Löfke et al., 2013](#)).

Additionally, we found evidence that fiber production can be genetically decoupled from the maturation of cell walls competent of generating contractile force. We imaged two molecular markers of functional tension wood G-layers: JIM14 immunolocalization of arabinogalactan proteins (including FLAs) and [XET](#) in gravistimulated stems of wild-type trees and trees with increased or decreased *ARK2* transcripts. Stems with decreased *ARK2* transcript abundance produce more fibers but are delayed in fiber maturation (as assayed by Jim14 and [XET](#) labeling) and display reduced gravibending. Stems with increased *ARK2* transcripts produce fewer fibers, but fiber maturation and gravibending are enhanced. Thus, force generation and gravibending can be genetically decoupled from fiber differentiation, *per se*. While we expect that the dramatic differences in fiber maturation among *ARK2* genotypes is a primary factor, undoubtedly other differences such as stem stiffness also contribute to the observed differences in gravibending among these genotypes.

We used [GA](#) treatment, *ARK2* transcript levels, and gravistimulation as perturbations of gene expression to model gene coexpression networks underlying tension wood formation. An unexpected finding using comparisons of differentially expressed gene transcripts across all treatments was that opposite wood undergoes a massive reprogramming of gene expression. While typically assumed to play a passive role in gravibending, these results suggest the possibility of an active role, perhaps through production of signals or metabolic contributions to gravitropism. To more fully extract information from the transcriptome data, gene modules were defined based on gene coexpression across wood types,

genotypes, and [GA](#) treatments. Each module was annotated and characterized based on correlations with wood phenotypes, [GA](#) response, ARK2 binding to genes within specific modules, correlations with wood properties, and enrichment of member genes in specific gene ontology categories. These annotations allowed us to not only identify gene modules of interest for further study, but also define relationships among modules and make inferences about mechanisms regulating xylem development. For example, of the three modules showing significant correlations with microfibril angle and cellulose crystallinity (traits strongly associated with tension wood), only two were correlated with [GA](#) treatment, potentially reflecting our experimental data showing the primary effect of [GA](#) was in promoting fiber development but not cell wall development. We were also able to dissect modules based on annotations, module membership (a measure of connectivity of a gene with other genes in the module), and differential expression across treatments. For example, *ARK2* showed only modest connectivity and differential expression across wood types. Along with the observation that ARK2 binds to large numbers of genes of diverse function, these properties suggest that ARK2 is not a “master regulator” but rather influences the expression of genes of different function, potentially to integrate different developmental processes. This would be consistent with reports of KNOX genes regulating both hormone-related as well as cell wall-related genes in other model species ([Sakamoto et al., 2001](#); [Mele et al., 2003](#); [Jasinski et al., 2005](#); [Bolduc and Hake, 2009](#); [Bolduc et al., 2012](#)).

The interaction of [GA](#) and ARK2 in regulating tension wood development was evident not only in experimental data, but also in coexpression analyses. A coexpression module was selected for dissection that showed significant correlations with tension wood properties and contained a large number of *FLAs* implicated in the tension wood development and function ([Lafargue et al., 2004](#); [Andersson-Gunneras et al., 2006](#); [Azri et al., 2014](#)). Interestingly, the expression of these *FLA* genes was differential across both wood types and *ARK2* genotypes in response to [GA](#), similar to what we observed in response to [GA](#) treatment of fiber production and maturation across *ARK2* genotypes. Taken together, these results are consistent with ARK2 negatively regulating [GA](#) levels, as has been reported in other species ([Sakamoto et al., 2001](#); [Hay et al., 2002](#); [Bolduc and Hake, 2009](#)), but also having an additional role in regulating cell differentiation and cell wall biosynthesis.

In conclusion, the results from these studies not only provide insights into the regulation of gravitropism and wood formation in angiosperm trees, but also demonstrate that the combination of experimental and computational approaches can be used to dissect complex developmental traits in these long-lived organisms. Challenges for future studies include determining the evolutionary relationships of graviperception and graviresponse mechanisms in woody versus herbaceous stems and roots and whether the mechanisms described here for *Populus* also function across the amazing diversity of angiosperm tree species.

## METHODS

---

### Replication

In all experiments, a minimum of three biological replicates were included for each treatment.

## Plant Growth

The genetic background of all trees utilized is hybrid aspen (*Populus alba* × *Populus tremula*) clone INRA 717-IB4. Representative *ARK2* transgenic genotypes were selected from those previously described and characterized ([Du et al., 2009](#)). The creation and characterization of the DR5:GUS reporter line was characterized and reported previously ([Spicer et al., 2013](#)). Plants were grown at ~22°C under continuous light provided by Philips TL830 and TL850 fluorescent bulbs. Plants used for time-lapse movies, immunolocalizations, [XET](#) labeling, GUS expression assays, and histology were transferred to soil (Sunshine Mix 4; SunGro Horticulture) in 0.5-liter pots, covered by a transparent lid (Super Sprouter), and adjusted to ambient humidity over the course of 2 weeks. Plants were used for experiments after 2 months growth in soil with water supplemented with Miracle Grow fertilizer using the concentration recommended by the manufacturer. For [GA](#) soil drench treatments, 50 mL of 0.01% [GA](#) (Sigma-Aldrich G-7645) in water was added to each pot to give an approximate concentration of 29 μmol [GA](#) in the soil. Plants were grown for four additional days after [GA](#) treatment prior to gravistimulation.

## Histology, Imaging, and Auxin Transport Measurement

Time-lapse movies were captured using Wingscape time-lapse digital cameras (Wingscapes; EBSCO Industries). Plants were positioned horizontally and imaged once every 10 min on the first day and then once per hour for 2 weeks. Quantification of stem lift and curvature was analyzed using custom R scripts, using data derived from digitized tracings of stems from individual frames taken from time-lapse movies. Tracings analyzed were from the base of the stem to the apex of curvature (defined as the basal point of tropism of the primary, herbaceous portion of the stem).

Stems were sectioned for histology using a Vibratome Series 1000 (Heath Company) to a thickness of 50 to 100 μm. Sections for anatomical assays were stained with astra blue and phloroglucinol ([Ruzin, 1999](#)) and visualized with a Leica DMB compound microscope using a Leica DFC450C digital camera with live image stitching using Leica Live Image Builder software.

For [XET](#) activity visualization, XXXG-SR was synthesized as previously described ([Nishikubo et al., 2007](#)). The previously described labeling protocol ([Nishikubo et al., 2007](#)) was modified by utilizing Vibratome sections rather than hand-sections and by blocking sections (25 mM MES, pH 5.5, 1% BSA, and 2% fish gelatin) prior to incubation with 4 μg/mL XXXG-SR in block. For estimation of background signal, sections were boiled for 10 min prior to blocking and incubation with XXXG-SR. After overnight incubation at room temperature, sections were rinsed four times with 25 mM MES and then stepped gradually into a wash solution of 15:1:4 ethanol:formic acid:water. After multiple changes of wash solutions, sections were stepped back to 25 mM MES prior to imaging on a Zeiss LSM 710 confocal

microscope.

The Pt-PIN3 antibody was raised against a conjugated peptide (DQREKEGPTGLNLKGSS-C) unique to paralogous *Populus* PIN3-like proteins Potri.008G129400 and Potri.010G112800 in rabbits and used at a dilution of 1:250. To assay specificity of the antibody, membrane proteins were extracted from both leaf and stem tissues of *P. alba* × *P. tremula* clone INRA 717-IB4. Tissues were ground in liquid nitrogen and suspended in an extraction buffer before extraction as previously described ([Abas and Luschnig, 2010](#)). Resulting pellets were frozen at -80°C and then thawed and subjected to a second extraction using transmembrane protein extraction reagent (FIVEphoton Biochemicals) according to the manufacturer's protocol.

Immunolocalizations were performed using Vibratome stem sections that were fixed at room temperature in formalin, acetic acid, and alcohol for 45 min under vacuum. Sections were then stepped to PBT (1× PBS with 0.2% Tween 20) and washed four times 15 min each. Sections were then blocked (1× PBS, 2% fish gelatin, 1% BSA, and 0.2% Tween 20) for 1 h prior to addition of the primary antibody. The JIM14 antibody was obtained from the Complex Carbohydrate Research Center (University of Georgia, Athens, GA) and used at a dilution of 1:500. After overnight incubation at 4°C, sections were washed four times in 1× PBT, blocked for 1 h, and probed with biotin-labeled antibodies (for JIM14, biotin-xx-goat-anti-rat IgG, Life Technologies A10517; for Pt-PIN3 biotin-xx-goat-anti-rabbit IgG, Life Technologies B2770) at 1:400 dilution. After overnight incubation at 4°C, sections were washed four times with PBT, blocked for 1 h, and 4 µL Streptavidin Alexa Flour-488 (Life Technologies [S11223](#)) added per milliliter of block. After 0.5 h incubation at room temperature, sections were washed four times with PBT prior to visualization on a Zeiss LSM 710 confocal microscope.

GUS staining was performed on 100- to 150-µm thick sections by vacuum infiltration of staining solution (100 mM sodium phosphate, pH 7, 10 mM EDTA, 0.1% Triton X-100, 0.5 mg/mL X-glucuronide, and 100 µg/mL chloramphenicol) followed by overnight incubation at 37°. Sections were cleared in 70% ethanol prior to imaging on a Leica DMLB compound microscope with Leica DFC450C digital camera and live image stitching using Leica Live Image Builder software.

Basipetal (toward the root) auxin transport was measured in stems of poplar seedlings in tissue culture ([Groover et al., 2006](#)) using a radio-tracer auxin transport assay adapted from *Arabidopsis thaliana* inflorescences ([Lewis and Muday, 2009](#)). Developmentally matched seedlings with consistent stem thickness were stripped of leaves and cut 20 and 40 mm from the shoot apex, forming a 20-mm section. These samples were inverted and placed into an open 0.5-mL microcentrifuge tube containing 200 µL 100 nM  $^3\text{H}$ -IAA (24 Ci/mmol; American Radiochemical) such that the apical cut end was submerged. Assay tubes were placed in a sealed box filled with water to prevent evaporation. After 18 h, the seedlings were removed and the apical 10 mm from the site of auxin application was removed and discarded. The next remaining 10-mm basal section was then divided into 2-mm segments and assayed for radioactivity in a Beckman LS6500 scintillation counter. The average and SE of  $^3\text{H}$ -IAA in each sample is reported relative to the distance to the

apical end.

## RNA-seq and ChIP-seq

Plants grown as described previously were transferred to 8-liter pots in Sunshine Mix 4 (SunGro Horticulture) and grown in a greenhouse in Placerville, CA without supplemental light for 3 months. For GA soil drench treatments, 0.01% GA in water was added to each pot to give an approximate concentration of 29 µm GA in the soil. Trees subjected to gravistimulation were placed horizontally 4 d after GA treatments were applied, and differentiating xylem for RNA-seq was harvested from all plants 2 d after gravistimulation commenced. For gravistimulated trees, bark was removed from the top (for tension wood) or bottom (for opposite wood) quarter of the stem and differentiating xylem harvested by light scraping with a sterile double-edged razor blade. For upright trees, the stem was randomly divided in half, and two xylem samples were independently harvested from opposing sides. For all trees, xylem was harvested from the twentieth leaf to the midpoint of the total length of the stem and flash-frozen in liquid nitrogen. Total RNA was isolated by grinding the tissue to a fine powder in liquid nitrogen, followed by extraction using Trizol (Life Technologies) using the manufacturer's suggested protocol. RNA samples were then treated with RNase-free DNase (Qiagen) prior to secondary isolation using the Qiagen RNeasy kit following the manufacturer's protocol. Quality and quantity of RNA was assessed using Qubit (Life Technologies) and Bioanalyzer (Agilent Technologies), respectively, prior to generation of RNA-seq libraries using the Illumina TruSeq Library Preparation Kit V2. Six samples were multiplexed into each lane of an Illumina HiSeq run to produce 50-bp single-end reads. ARK2 ChIP-seq data were produced and analyzed as previously described (Liu et al., 2015) and are available as NCBI SRI accession SRP0533 or through popGENIE (<http://popgenie.org/> ).

## Bioinformatics

For each RNA-seq library, contamination from adaptor sequences was removed using scythe V0.95 (<https://github.com/vsbuffalo/scythe> ), and sequenced reads were trimmed using sickle (Joshi and Fass, 2011) with default settings. Sequenced reads were then mapped to the *Populus* genome assembly V3.0 (<http://www.phytozome.net/poplar.php> ) using TopHat v2.0.6 (Trapnell et al., 2009), and reads for *Populus* V3.0 gene models were counted using HTseq (Trapnell et al., 2009) version 0.5.4p1. Gene expression levels were calculated as reads per kilobase per million reads using the TMM normalization method in the package edgeR V3.6.8 (Robinson et al., 2010). All statistical analyses were implemented in R (R Development Core Team, 2014) unless stated otherwise.

Coexpression and module analyses were performed using functions from the R package WGCNA V1.41-1 (Langfelder and Horvath, 2008) and publically available scripts (<http://labs.genetics.ucla.edu/horvath/CoexpressionNetwork/Rpackages/WGCNA/> ). Briefly, coexpression relationships between genes were summarized as an adjacency matrix and raised to the soft threshold power of eight. The soft threshold power was determined based on a greater 80% model

fit to scale-free topology and low mean connectivity. Coexpression modules were defined as clusters of highly interconnected genes and calculated using hierarchical clustering of dissimilarity of the topological overlap measure. Hierarchical clustering was performed using dynamic tree cutting with a minimum module size of 500 and a cut height of 0.998, and closely related modules (0.3) based on module eigengene values were collapsed. Module stability was assessed by resampling 75% of the RNA-seq libraries and rerunning the coexpression analysis 20 times ([Langfelder and Horvath, 2012](#)).

Traits were related to modules using module eigengene values. Module correlations for experimental treatments such as *ARK2* genotype, wood type, and [GA](#) treatments were tested using ANOVA, and wood chemistry phenotypes were tested using Fisher's exact tests. Enrichment of *ARK2* [ChIP-seq](#) binding in coexpression modules was determined based on a one-tailed hypergeometric distribution. Hub genes in the pink module were identified as genes that had high gene significance with wood type and high module membership in the pink module. Gene significance was calculated as the correlation between gene expression (reads per kilobase per million reads) and wood type. Module membership was calculated as the correlation between gene expression and module eigengene values for the pink module.

Functional enrichment of coexpression modules was based on [GO](#) enrichment and calculated using Arabidopsis best BLAST hit of *Populus* gene models. [GO](#) analysis was performed using Arabidopsis [GO](#) annotations because categories related to relevant categories (including meristem, shoot development, hormones, cell wall and cellulose) have limited annotation in *Populus*. Analyses were performed using the Bioconductor package GOstats V2.30.0 ([Falcon and Gentleman, 2007](#)) with P < 0.01.

## Wood Chemistry and Cell Wall Phenotyping

A micro-Klason method was applied to quantify lignin and cell wall carbohydrates ([Coleman et al., 2007](#)). Approximately 200 mg of extracted, oven-dried wood was reacted in a 125-mL serum bottle with 3 mL of 20°C 72% (w/w) sulfuric acid (H<sub>2</sub>SO<sub>4</sub>), with thorough mixing with a glass rod for 1 min every 10 min, followed by mixing for 15 s every 10 min thereafter. After 2 h, 112 mL deionized water was added to the reaction. The serum bottles were then sealed and immediately autoclaved at 121°C for 60 min. Sugar standards were subjected to the same treatment. Samples were allowed to cool and settle at 4°C and were vacuum-filtered through preweighed medium coarseness (M) sintered-glass crucibles. Each sample was washed (and the serum bottle also rinsed) with 200 mL warm (~50°C) deionized water to remove residual acid and sugars and dried overnight at 105°C. The dry crucibles were reweighed to determine Klason lignin (acid-insoluble lignin) gravimetrically. The filtrate was then analyzed for acid-soluble lignin by absorbance at 205 nm using a UV/Vis spectrometer. Samples had to be diluted with 4% H<sub>2</sub>SO<sub>4</sub> to reach an absorbance value between 0.2 and 0.7. The concentrations for neutral cell wall-associated carbohydrates (glucose, xylose, mannose, galactose, rhamnose, and arabinose) in the hydrolyzate were determined using HPLC. Prior to injection, samples were filtered through 0.45-μm HV filters (Millipore). The samples for HPLC runs were prepared by exact weights of ~950 mg hydrolyzate + 50 mg fucose as the internal standard. The concentrations of sugar monosaccharides were determined

using a Dionex HPLC system (DX-600) equipped with an ion exchange PA1 column (Dionex), a pulsed amperometric detector with a gold electrode, and a SpectraAS3500 auto injector (Spectra-Physics). The column was equilibrated with 250 mM NaOH and eluted with deionized water at flow rate of 1 mL/min. Total lignin content was calculated as the sum of the Klason lignin and soluble lignin fractions. Lignin and cell wall sugar content was determined as a percentage of dry wood, based on the initial weight of the extract-free wood sample analyzed.

Microfibril angle and cell wall crystallinity were determined by x-ray diffraction using a Bruker D8 Discover x-ray diffraction unit equipped with an area array detector (GADDS) on the radial face of the wood section precision cut (1.6 mm) from the growing stem isolated from the tension wood and opposite wood sections isolated from 10 cm above the root collar. Wide-angle diffraction was used in transmission mode, and the measurements were performed with CuK $\alpha$ 1 radiation ( $\lambda = 1.54 \text{ \AA}$ ), the x-ray source fit with a 0.5-mm collimator, and the scattered photon collected by a GADDS detector. Both the x-ray source and the detector were set to  $\theta = 0^\circ$  for microfibril angle determination, while the  $2\theta$  (source) was set to  $17^\circ$  for wood crystallinity determination. The average T-value of the two 002 diffraction arc peaks was used for microfibril angle calculations, as per the method of [Ukainetz et al. \(2008\)](#), while crystallinity was determined by mathematically fitting the data using the method of [Coleman et al. \(2007\)](#). Crystallinity measures were precalibrated by capturing diffractograms of pure *Acetobacter xylinum* bacterial cellulose (known to be 87% crystalline).

Fiber length was analyzed using the woody material isolated from the tension wood and opposite wood side of each specimen, according to [Park et al. \(2008\)](#). In brief, each sample was macerated in a solution consisting of 30% hydrogen peroxide and glacial acetic acid in a 1:1 ratio (Franklin solution) at 70°C for 48 h. Following the reaction, the remaining fibrous material was washed with deionized water until the samples were neutralized. Subsamples were resuspended in 10 mL deionized, distilled water and analyzed on a fiber quality analyzer (FQA; Optest Equipment). Fiber length was recorded in millimeters.

## Accession Numbers

The sequences associated with RNA-seq experiments are deposited in NCBI SRA under BioProject PRJNA284622. The sequences associated with [ChIP-seq](#) of ARK2 are deposited in NCBI SRA under accession SRP0533. Phytozome accession numbers for *Populus* orthologs of *Arabidopsis* genes discussed in reference to gene module dissection are as follows: *MYB52* (Potri.012G039400), *MYB85* (Potri.015G129100), *KNAT6* (Potri.010G043500), *KNAT7* (Potri.001G112200), *BLH4* (Potri.007G032700), *VND1* (Potri.007G014400), *PIN1* (Potri.015G038700), *PIN3* (Potri.015G038700 and Potri.008G129400), *GA20-Oxidase* (Potri.015G134600), *IRREGULAR XYLEM* genes (Potri.004G117200, Potri.009G042500, and Potri.001G248700), *CLE13-like* (Potri.008G115600), and *SCARECROW-like 8* (Potri.004G078800).

## Supplemental Data

- Supplemental Figure 1.** Quantification of gravitropic bending and longitudinal growth in *ARK2* genotypes during a 2-week gravistimulus trial.
- Supplemental Figure 2.** Opposite wood histology.
- Supplemental Figure 3.** JIM14 immunolocalization of arabinogalactan protein epitopes in opposite wood of *ARK2* genotypes and negative control showing background labeling.
- Supplemental Figure 4.** Imaging of *XET* activity in opposite wood of *ARK2* genotypes.
- Supplemental Figure 5.** PIN3 and control immunolocalization.
- Supplemental Figure 6.** PIN3 quantification in tension wood and localization in opposite wood.
- Supplemental Figure 7.** *GA* effects on DR5:GUS expression in upright stems and on gravibending in *ARK2* genotypes.
- Supplemental Figure 8.** JIM14 immunolocalization for stem sections of trees treated with *GA*.
- Supplemental Figure 9.** In situ imaging of *XET* activity in stems of trees treated with *GA*.
- Supplemental Figure 10.** Differential expression of genes in opposite wood versus tension wood and normal wood.
- Supplemental Figure 11.** Characterization of gene coexpression network modules.
- Supplemental Figure 12.** Quantification of wood property and chemistry traits for wood types within each *ARK2* genotype.
- Supplemental Movie 1.** Time-lapse movie of wild-type poplar undergoing gravitropic bending.
- Supplemental Movie 2.** Time-lapse movie of OE-ARK2 poplar undergoing gravitropic bending.
- Supplemental Movie 3.** Time-lapse movie of miRNA-ARK2 poplar undergoing gravitropic bending.
- Supplemental Data Set 1.** Gene module memberships and statistics for poplar genes expressed during wood formation.
- Supplemental Data Set 2.** Gene Ontology enrichment analysis for gene modules.

## Supplementary Material

---

### Supplemental Data

[supp\\_27\\_10\\_2800\\_index.html](#) (1.8KB, html)

## Author Profile

[supp\\_27\\_10\\_2800\\_v2\\_index.html](#) (2.8KB, html)

## Acknowledgments

---

This work was supported by Grants 2011-67013-30062 and 2015-67013-22891 from USDA AFRI to A.G. and V.F. M.Z. is supported by NSF Postdoctoral Research Fellowship in Biology Grant IOS-1402064. G.K.M. was supported by NASA Grant NNX09AK82G. This work used the Vincent J. Coates Genomics Sequencing Laboratory at UC Berkeley, supported by NIH S10 Instrumentation Grants S10RR029668 and S10RR027303. We thank Courtney Castle and Annie Mix for assistance in plant propagation and care. We thank Julin Maloof, Daniel Fulop, and Christine Palmer for guidance on computational analyses of stem movements.

## AUTHOR CONTRIBUTIONS

---

A.G., S.G., and V.F. conceived of this research program. S.G. performed time-lapse videos, immunolocalizations, Lugol staining, GUS staining, histology, and fiber counts. M.Z. performed bioinformatics analyses with guidance from V.F., A.G., S.G., and M.Z. performed RNA-seq experiments. S.D.M. and F.H. contributed wood chemistry, ultrastructure, and fiber data. G.K.M. and D.R.L. contributed auxin transport assays. F.M.I. and H.B. synthesized the [XET](#) substrate. A.G. performed [XET](#) imaging and wrote the article.

## Glossary

### GA

gibberellic acid

### XET

xyloglucan endotransglycosylase

### ChIP-seq

chromatin immunoprecipitation sequencing

### GO

Gene Ontology

## Footnotes

---

[OPEN] Articles can be viewed online without a subscription.

## References

---

1. Abas L., Luschnig C. (2010). Maximum yields of microsomal-type membranes from small amounts of plant material without requiring ultracentrifugation. *Anal. Biochem.* 401: 217–227. [[DOI](#)] [[PMC free article](#)] [[PubMed](#)] [[Google Scholar](#)]
2. Andersson-Gunnerås S., Hellgren J.M., Björklund S., Regan S., Moritz T., Sundberg B. (2003). Asymmetric expression of a poplar ACC oxidase controls ethylene production during gravitational induction of tension wood. *Plant J.* 34: 339–349. [[DOI](#)] [[PubMed](#)] [[Google Scholar](#)]
3. Andersson-Gunneras S., Mellerowicz E.J., Love J., Segerman B., Ohmiya Y., Coutinho P.M., Nilsson P., Henrissat B., Moritz T., Sundberg B. (2006). Biosynthesis of cellulose-enriched tension wood in *Populus*: global analysis of transcripts and metabolites identifies biochemical and developmental regulators in secondary wall biosynthesis. *Plant J.* 45: 144–165. [[DOI](#)] [[PubMed](#)] [[Google Scholar](#)]
4. Azri W., Ennajah A., Nasr Z., Woo S.Y., Khaldi A. (2014). Transcriptome profiling the basal region of poplar stems during the early gravitropic response. *Biol. Plant.* 58: 55–63. [[Google Scholar](#)]
5. Belles-Boix E., Hamant O., Witiak S.M., Morin H., Traas J., Pautot V. (2006). KNAT6: An *Arabidopsis* homeobox gene involved in meristem activity and organ separation. *Plant Cell* 18: 1900–1907. [[DOI](#)] [[PMC free article](#)] [[PubMed](#)] [[Google Scholar](#)]
6. Bjorklund S., Antti H., Udstrand I., Moritz T., Sundberg B. (2007). Cross-talk between gibberellin and auxin in development of *Populus* wood: gibberellin stimulates polar auxin transport and has a common transcriptome with auxin. *Plant J.* 52: 499–511. [[DOI](#)] [[PubMed](#)] [[Google Scholar](#)]
7. Bolduc N., Hake S. (2009). The maize transcription factor KNOTTED1 directly regulates the gibberellin catabolism gene *ga2ox1*. *Plant Cell* 21: 1647–1658. [[DOI](#)] [[PMC free article](#)] [[PubMed](#)] [[Google Scholar](#)]
8. Bolduc N., Yilmaz A., Mejia-Guerra M.K., Morohashi K., O'Connor D., Grotewold E., Hake S. (2012). Unraveling the KNOTTED1 regulatory network in maize meristems. *Genes Dev.* 26: 1685–1690. [[DOI](#)] [[PMC free article](#)] [[PubMed](#)] [[Google Scholar](#)]
9. Chuck G., Lincoln C., Hake S. (1996). KNAT1 induces lobed leaves with ectopic meristems when overexpressed in *Arabidopsis*. *Plant Cell* 8: 1277–1289. [[DOI](#)] [[PMC free article](#)] [[PubMed](#)] [[Google Scholar](#)]

10. Clair B., Alméras T., Pilate G., Jullien D., Sugiyama J., Riekel C. (2011). Maturation stress generation in Poplar tension wood studied by synchrotron radiation microdiffraction. *Plant Physiol.* 155: 562–570. [[DOI](#)] [[PMC free article](#)] [[PubMed](#)] [[Google Scholar](#)]
11. Clair B., Almeras T., Yamamoto H., Okuyama T., Sugiyama J. (2006). Mechanical behavior of cellulose microfibrils in tension wood, in relation with maturation stress generation. *Biophys. J.* 91: 1128–1135. [[DOI](#)] [[PMC free article](#)] [[PubMed](#)] [[Google Scholar](#)]
12. Coleman H.D., Canam T., Kang K.Y., Ellis D.D., Mansfield S.D. (2007). Over-expression of UDP-glucose pyrophosphorylase in hybrid poplar affects carbon allocation. *J. Exp. Bot.* 58: 4257–4268. [[DOI](#)] [[PubMed](#)] [[Google Scholar](#)]
13. Cronshaw J., Morey P. (1968). The effect of plant growth substances on the development of tension wood in horizontally inclined stems of *Acer rubrum* seedlings. *Protoplasma* 65: 379–391. [[Google Scholar](#)]
14. Cronshaw J., Morey P.R. (1965). Induction of tension wood by 2,3,5-tri-iodobenzoic acid. *Nature* 205: 816–818. [[Google Scholar](#)]
15. Déjardin A., Leplé J.C., Lesage-Descaves M.C., Costa G., Pilate G. (2004). Expressed sequence tags from Poplar wood tissues: A comparative analysis from multiple libraries. *Plant Biol. (Stuttg.)* 6: 55–64. [[DOI](#)] [[PubMed](#)] [[Google Scholar](#)]
16. Du J., Mansfield S.D., Groover A.T. (2009). The *Populus* homeobox gene *ARBORKNOX2* regulates cell differentiation during secondary growth. *Plant J.* 60: 1000–1014. [[DOI](#)] [[PubMed](#)] [[Google Scholar](#)]
17. Eriksson M.E., Israelsson M., Olsson O., Moritz T. (2000). Increased gibberellin biosynthesis in transgenic trees promotes growth, biomass production and xylem fiber length. *Nat. Biotechnol.* 18: 784–788. [[DOI](#)] [[PubMed](#)] [[Google Scholar](#)]
18. Falcon S., Gentleman R. (2007). Using GOstats to test gene lists for GO term association. *Bioinformatics* 23: 257–258. [[DOI](#)] [[PubMed](#)] [[Google Scholar](#)]
19. Friml J., Wisniewska J., Benkova E., Mendgen K., Palme K. (2002). Lateral relocation of auxin efflux regulator PIN3 mediates tropism in *Arabidopsis*. *Nature* 415: 806–809. [[DOI](#)] [[PubMed](#)] [[Google Scholar](#)]
20. Goswami L., Dunlop J.W.C., Jungnikl K., Eder M., Gierlinger N., Coutand C., Jeronimidis G., Fratzl P., Burgert I. (2008). Stress generation in the tension wood of poplar is based on the lateral swelling power of the G-layer. *Plant J.* 56: 531–538. [[DOI](#)] [[PubMed](#)] [[Google Scholar](#)]
21. Groover A., Mansfield S., DiFazio S., Dupper G., Fontana J., Millar R., Wang Y. (2006). The *Populus*

homeobox gene *ARBORKNOX1* reveals overlapping mechanisms regulating the shoot apical meristem and the vascular cambium. *Plant Mol. Biol.* 61: 917–932. [\[DOI\]](#) [\[PubMed\]](#) [\[Google Scholar\]](#)

22. Hay A., Kaur H., Phillips A., Hedden P., Hake S., Tsiantis M. (2002). The gibberellin pathway mediates KNOTTED1-type homeobox function in plants with different body plans. *Curr. Biol.* 12: 1557–1565.

[\[DOI\]](#) [\[PubMed\]](#) [\[Google Scholar\]](#)

23. Hay A., Tsiantis M. (2010). KNOX genes: versatile regulators of plant development and diversity. *Development* 137: 3153–3165. [\[DOI\]](#) [\[PubMed\]](#) [\[Google Scholar\]](#)

24. Hellgren J.M., Olofsson K., Sundberg B. (2004). Patterns of auxin distribution during gravitational induction of reaction wood in poplar and pine. *Plant Physiol.* 135: 212–220. [\[DOI\]](#) [\[PMC free article\]](#) [\[PubMed\]](#) [\[Google Scholar\]](#)

25. Israelsson M., Sundberg B., Moritz T. (2005). Tissue-specific localization of gibberellins and expression of gibberellin-biosynthetic and signaling genes in wood-forming tissues in aspen. *Plant J.* 44: 494–504. [\[DOI\]](#) [\[PubMed\]](#) [\[Google Scholar\]](#)

26. Jasinski S., Piazza P., Craft J., Hay A., Woolley L., Rieu I., Phillips A., Hedden P., Tsiantis M. (2005). KNOX action in *Arabidopsis* is mediated by coordinate regulation of cytokinin and gibberellin activities. *Curr. Biol.* 15: 1560–1565. [\[DOI\]](#) [\[PubMed\]](#) [\[Google Scholar\]](#)

27. Joshi N.A., Fass J.N. (2011). Sickle: A sliding-window, adaptive, quality-based trimming tool for FastQ files (version 1.200). Available at <https://github.com/najoshi/sickle>.

28. Knox J.P., Linstead P.J., Cooper J.P.C., Roberts K. (1991). Developmentally regulated epitopes of cell surface arabinogalactan proteins and their relation to root tissue pattern formation. *Plant J.* 1: 317–326. [\[DOI\]](#) [\[PubMed\]](#) [\[Google Scholar\]](#)

29. Lafarguette F., Leplé J.-C., Déjardin A., Laurans F., Costa G., Lesage-Descauses M.-C., Pilate G. (2004). Poplar genes encoding fasciclin-like arabinogalactan proteins are highly expressed in tension wood. *New Phytol.* 164: 107–121. [\[DOI\]](#) [\[PubMed\]](#) [\[Google Scholar\]](#)

30. Langfelder P., Horvath S. (2008). WGCNA: an R package for weighted correlation network analysis. *BMC Bioinformatics* 9: 559. [\[DOI\]](#) [\[PMC free article\]](#) [\[PubMed\]](#) [\[Google Scholar\]](#)

31. Langfelder P., Horvath S. (2012). Fast R functions for robust correlations and hierarchical clustering. *J. Stat. Softw.* 46: i11. [\[PMC free article\]](#) [\[PubMed\]](#) [\[Google Scholar\]](#)

32. Leach R.W.A., Wareing P.F. (1967). Distribution of auxin in horizontal woody stems in relation to gravimorphism. *Nature* 214: 1025–1027. [\[Google Scholar\]](#)

33. Lev-Yudan S., Aloni R. (1995). Differentiation of the ray system in woody plants. *Bot. Rev.* 61: 45–84. [[Google Scholar](#)]
34. Lewis D.R., Muday G.K. (2009). Measurement of auxin transport in *Arabidopsis thaliana*. *Nat. Protoc.* 4: 437–451. [[DOI](#)] [[PubMed](#)] [[Google Scholar](#)]
35. Little C.H.A., Savidge R.A. (1987). The role of plant growth regulators in forest tree cambial growth. *Plant Growth Regul.* 6: 137–169. [[Google Scholar](#)]
36. Liu L., Ramsay T., Zinkgraf M., Sundell D., Street N.R., Filkov V., and Groover A. (2015). A resource for characterizing genome-wide binding and putative target genes of transcription factors expressed during secondary growth and wood formation in *Populus*. *Plant J.* 82: 887–898. [[DOI](#)] [[PubMed](#)] [[Google Scholar](#)]
37. Liu Y., You S., Taylor-Teeple M., Li W.L., Schuetz M., Brady S.M., Douglas C.J. (2014). BEL1-LIKE HOMEO DOMAIN6 and KNOTTED ARABIDOPSIS THALIANA7 interact and regulate secondary cell wall formation via repression of REVOLUTA. *Plant Cell* 26: 4843–4861. [[DOI](#)] [[PMC free article](#)] [[PubMed](#)] [[Google Scholar](#)]
38. Löfke C., Zwiewka M., Heilmann I., Van Montagu M.C.E., Teichmann T., Friml J. (2013). Asymmetric gibberellin signaling regulates vacuolar trafficking of PIN auxin transporters during root gravitropism. *Proc. Natl. Acad. Sci. USA* 110: 3627–3632. [[DOI](#)] [[PMC free article](#)] [[PubMed](#)] [[Google Scholar](#)]
39. MacMillan C.P., Mansfield S.D., Stachurski Z.H., Evans R., Southerton S.G. (2010). Fasciclin-like arabinogalactan proteins: specialization for stem biomechanics and cell wall architecture in *Arabidopsis* and *Eucalyptus*. *Plant J.* 62: 689–703. [[DOI](#)] [[PubMed](#)] [[Google Scholar](#)]
40. Mauriat M., Moritz T. (2009). Analyses of GA20ox and GID1 over-expressing aspen suggest that gibberellins play two distinct roles in wood formation. *Plant J.* 58: 989–1003. [[DOI](#)] [[PubMed](#)] [[Google Scholar](#)]
41. Mele G., Ori N., Sato Y., Hake S. (2003). The knotted1-like homeobox gene BREVIPE DICELLUS regulates cell differentiation by modulating metabolic pathways. *Genes Dev.* 17: 2088–2093. [[DOI](#)] [[PMC free article](#)] [[PubMed](#)] [[Google Scholar](#)]
42. Mellerowicz E.J., Gorshkova T.A. (2012). Tensional stress generation in gelatinous fibres: a review and possible mechanism based on cell-wall structure and composition. *J. Exp. Bot.* 63: 551–565. [[DOI](#)] [[PubMed](#)] [[Google Scholar](#)]
43. Mellerowicz E.J., Immerzeel P., Hayashi T. (2008). Xyloglucan: The molecular muscle of trees. *Ann. Bot. (Lond.)* 102: 659–665. [[DOI](#)] [[PMC free article](#)] [[PubMed](#)] [[Google Scholar](#)]

44. Nakamura T., Saotome M., Ishiguro Y., Itoh R., Higurashi S., Hosono M., Ishii Y. (1994). The effects of GA3 on weeping of growing shoots of the Japanese cherry, *Prunus spachiana*. Plant Cell Physiol. 35: 523–527. [[Google Scholar](#)]
45. Nishikubo N., Awano T., Banasiak A., Bourquin V., Ibatullin F., Funada R., Brumer H., Teeri T.T., Hayashi T., Sundberg B., Mellerowicz E.J. (2007). Xyloglucan endo-transglycosylase (XET) functions in gelatinous layers of tension wood fibers in poplar—a glimpse into the mechanism of the balancing act of trees. Plant Cell Physiol. 48: 843–855. [[DOI](#)] [[PubMed](#)] [[Google Scholar](#)]
46. Norberg P.H., Meier H. (1996). Physical and chemical properties of gelatinous layer in tension wood fibres of aspen (*Populus tremula* L.). Holzforschung 20: 174–178. [[Google Scholar](#)]
47. Park J.Y., Canam T., Kang K.Y., Ellis D.D., Mansfield S.D. (2008). The effects of over-expression of an Arabidopsis sucrose phosphate synthase (SPS) gene on plant growth and fibre development. Transgenic Res. 17: 181–192. [[DOI](#)] [[PubMed](#)] [[Google Scholar](#)]
48. R Development Core Team (2014). R: A Language and Environment for Statistical Computing. (Vienna, Austria Foundation for Statistical Computing).
49. Ragni L., Belles-Boix E., Günl M., Pautot V. (2008). Interaction of KNAT6 and KNAT2 with BREVIPEDICELLUS and PENNYWISE in Arabidopsis Inflorescences. Plant Cell 20: 888–900. [[DOI](#)] [[PMC free article](#)] [[PubMed](#)] [[Google Scholar](#)]
50. Robinson M., McCarthy D.J., Smyth G. (2010). edgeR: a Bioconductor package for differential expression analysis of digital gene expression data. Bioinformatics 26: 139–140. [[DOI](#)] [[PMC free article](#)] [[PubMed](#)] [[Google Scholar](#)]
51. Ruelle J. (2014). Morphology, Anatomy and Ultrastructure of Reaction Wood. (Berlin, Heidelberg, Germany: Springer-Verlag; ). [[Google Scholar](#)]
52. Ruzin S. (1999). Plant Microtechnique and Microscopy. (New York: Oxford University Press; ). [[Google Scholar](#)]
53. Sakamoto T., Kamiya N., Ueguchi-Tanaka M., Iwahori S., Matsuoka M. (2001). KNOX homeodomain protein directly suppresses the expression of a gibberellin biosynthetic gene in the tobacco shoot apical meristem. Genes Dev. 15: 581–590. [[DOI](#)] [[PMC free article](#)] [[PubMed](#)] [[Google Scholar](#)]
54. Schrader J., Baba K., May S.T., Palme K., Bennett M., Bhalerao R.P., Sandberg G. (2003). Polar auxin transport in the wood-forming tissues of hybrid aspen is under simultaneous control of developmental and environmental signals. Proc. Natl. Acad. Sci. USA 100: 10096–10101. [[DOI](#)] [[PMC free article](#)] [[PubMed](#)] [[Google Scholar](#)]

55. Sinnott E.W. (1952). Reaction wood and the regulation of tree form. Am. J. Bot. 39: 69–78. [[Google Scholar](#) ]
56. Spicer R., Tisdale-Orr T., Talavera C. (2013). Auxin-responsive DR5 promoter coupled with transport assays suggest separate but linked routes of auxin transport during woody stem development in *Populus*. PLoS One 8: e72499. [[DOI](#) ] [[PMC free article](#)] [[PubMed](#)] [[Google Scholar](#) ]
57. Taylor-Teeple M., et al. (2015). An *Arabidopsis* gene regulatory network for secondary cell wall synthesis. Nature 517: 571–575. [[DOI](#) ] [[PMC free article](#)] [[PubMed](#)] [[Google Scholar](#) ]
58. Timell T.E. (1986). Compression Wood in Gymnosperms, Vol 2. (Heidelberg, Germany: Springer-Verlag; ). [[Google Scholar](#) ]
59. Trapnell C., Pachter L., Salzberg S.L. (2009). TopHat: discovering splice junctions with RNA-Seq. Bioinformatics 25: 1105–1111. [[DOI](#) ] [[PMC free article](#)] [[PubMed](#)] [[Google Scholar](#) ]
60. Ukrainetz N.K., Kang K.-Y., Aitken S.N., Stoehr M., Mansfield S.D. (2008). Heritability and phenotypic and genetic correlations of coastal Douglas fir (*Pseudotsuga menziesii*) wood quality traits. Can. J. For. Res. 38: 1536–1546. [[Google Scholar](#) ]
61. Venglat S.P., Dumonceaux T., Rozwadowski K., Parnell L., Babic V., Keller W., Martienssen R., Selvaraj G., Datla R. (2002). The homeobox gene BREVIPEDICELLUS is a key regulator of inflorescence architecture in *Arabidopsis*. Proc. Natl. Acad. Sci. USA 99: 4730–4735. [[DOI](#) ] [[PMC free article](#)] [[PubMed](#)] [[Google Scholar](#) ]
62. Willige B.C., Isono E., Richter R., Zourelidou M., Schwechheimer C. (2011). Gibberellin regulates PIN-FORMED abundance and is required for auxin transport-dependent growth and development in *Arabidopsis thaliana*. Plant Cell 23: 2184–2195. [[DOI](#) ] [[PMC free article](#)] [[PubMed](#)] [[Google Scholar](#) ]
63. Wilson B.F., Archer R.R. (1977). Reaction wood: Induction and mechanical action. Annu. Rev. Plant Physiol. 28: 23–43. [[Google Scholar](#) ]
64. Zhong R., Lee C., Zhou J., McCarthy R.L., Ye Z.-H. (2008). A Battery of transcription factors involved in the regulation of secondary cell wall biosynthesis in *Arabidopsis*. Plant Cell 20: 2763–2782. [[DOI](#) ] [[PMC free article](#)] [[PubMed](#)] [[Google Scholar](#) ]
65. Zhong R., Ye Z.-H. (2013). Transcriptional regulation of wood formation in tree species. In Cellular Aspects of Wood Formation, Vol. 20, Fromm J., ed (Heidelberg, Germany: Springer Berlin; ), pp. 141–158. [[Google Scholar](#) ]
66. Zhou J., Lee C., Zhong R., Ye Z.-H. (2009). MYB58 and MYB63 are transcriptional activators of the lignin biosynthetic pathway during secondary cell wall formation in *Arabidopsis*. Plant Cell 21: 248–266.

## Associated Data

*This section collects any data citations, data availability statements, or supplementary materials included in this article.*

## Supplementary Materials

### Supplemental Data

[supp\\_27\\_10\\_2800\\_index.html](#) (1.8KB, html)

[supp\\_tpc.15.00531\\_TPC2015-00531-RAR1\\_Supplemental\\_Data.pdf](#) (4.3MB, pdf)

[supp\\_tpc.15.00531\\_TPC2015-00531-RAR1\\_Supplemental\\_Data\\_set\\_1.xlsx](#) (10.6MB, xlsx)

[supp\\_tpc.15.00531\\_TPC2015-00531-RAR1\\_Supplemental\\_Data\\_set\\_2.xlsx](#) (462.8KB, xlsx)

[Download video file](#) (8MB, mov)

[Download video file](#) (7.7MB, mov)

[Download video file](#) (5.8MB, mov)

[supp\\_tpc.15.00531\\_TPC2015-00531-RAR1\\_Supplemental\\_Movie\\_Legends.docx](#) (16KB, docx)

### Author Profile

[supp\\_27\\_10\\_2800\\_v2\\_index.html](#) (2.8KB, html)

---

Articles from The Plant Cell are provided here courtesy of **Oxford University Press**